TU/e EINDHOVEN UNIVERSITY OF TECHNOLOGY

Eindhoven University of Technology

MASTER

Hydrogen passivation of N:GaAs studied using cross-sectional scanning tunneling microscopy

Tjeertes, Douwe

Award date:
2019

Link to publication

Disclaimer
This document contains a student thesis (bachelor's or master's), as authored by a student at Eindhoven University of Technology. Student theses are made available in the TU/e repository upon obtaining the required degree. The grade received is not published on the document as presented in the repository. The required complexity or quality of research of student theses may vary by program, and the required minimum study period may vary in duration.

General rights
Copyright and moral rights for the publications made accessible in the public portal are retained by the authors and/or other copyright owners and it is a condition of accessing publications that users recognise and abide by the legal requirements associated with these rights.

- Users may download and print one copy of any publication from the public portal for the purpose of private study or research.
- You may not further distribute the material or use it for any profit-making activity or commercial gain

Department of Applied Physics
Photonics and Semiconductor Nanophysics

Hydrogen passivation of N:GaAs studied using cross-sectional scanning tunneling microscopy

Master Thesis

Douwe Tjeertes

Supervisors:
dr. C.M. Krammel
prof. dr. P.M. Koenraad

Eindhoven, November 2018

Abstract

Introduction of a few percent N in GaAs causes a large reduction of its bandgap. This effect can be passivated by post-growth introduction of hydrogen into the material, the bandgap will then return to the value of N-free GaAs. Hydrogen is incorporated in the material in the form of two different NH-complexes, N-2H and N-3H. N-2H is responsible for the restoration of the bandgap, while N-3H influences the strain in the material. These NH-complexes can be removed again by annealing the samples either above 250°C, to remove the N-3H, or 330°C, to remove the N-2H. The complexes can also be removed at a local scale, either by laser irradiation or scanning near-field microscopy. This completely reverses the effects of the passivation, which allows for the creation of nano-structures such as quantum dots and nano wires. With cross-sectional scanning tunneling microscopy it should be possible to directly study the NH-complexes at the atomic scale for the first time.

Hydrogen passivated N:GaAs samples for XSTM measurements were obtained externally, but passivation trials have also been performed at the TU/e on N:GaAs and Sb:GaAs samples. For low dose exposure to a hydrogen plasma minimal change was observed in both photoluminescence (PL) and x-ray diffraction (XRD) measurements. The N:GaAs sample did show a decrease in the PL peak ratio between the N:GaAs and GaAs peak, indicating a partial passivation of the N:GaAs layer. After a second, higher dose exposure, both samples exhibited a significant change. Post-passivation annealing of the samples did not restore their properties from before the exposure to the hydrogen plasma. This is most likely a result of an etching of the top layers of both samples.

Cross-sectional scanning tunneling microscopy was performed on hydrogen passivated N:GaAs samples. We classified three features, two of which have never been seen before on non-passivated N:GaAs. The first feature is a N atom adsorbed on the surface. The other two are related to NH-complexes and can be switched or modified by taking spectroscopy curves at their location. Whether the features are N-2H or N-3H related could not be determined within this research.

Contents

Contents

1 Motivation **1**

2 Introduction **3**
- 2.1 Iso-electronic Impurities . . . 3
- 2.2 Hydrogen Passivation in Semiconductors . . . 4
- 2.3 Effects of Hydrogen Passivation on N:GaAs . . . 4
- 2.4 Functional Passivation . . . 6

3 Theory **7**
- 3.1 Scanning Tunneling Microscopy . . . 7
- 3.2 DOS and LDOS of Semiconductors . . . 8
- 3.3 Tunneling Theory for STM . . . 8
- 3.4 Topographic and Electronic Contrast in STM . . . 10
- 3.5 STM on (110) surfaces . . . 10
- 3.6 XSTM on N:GaAs . . . 11

4 Experimental Methods **13**
- 4.1 Tip Induced Band Bending . . . 13
- 4.2 Scanning Tunneling Spectroscopy . . . 14
- 4.3 STM Setup . . . 14
- 4.4 Sample Preparation . . . 16
- 4.5 Tip Preparation . . . 16
- 4.6 Other Measurement Setups . . . 17
  - 4.6.1 Photoluminescence . . . 17
  - 4.6.2 X-ray Diffraction . . . 17

5 Sample preparation and characterization **18**
- 5.1 Samples . . . 18
- 5.2 Hydrogen Passivation Setup and Conditions . . . 19
- 5.3 Hydrogen Passivation Simulations . . . 20
- 5.4 Photoluminescence . . . 21
  - 5.4.1 Sample 2131 . . . 21
  - 5.4.2 Sample 2233 . . . 21
- 5.5 Conclusion . . . 22

6 Hydrogen passivation tests at TU/e **23**
- 6.1 Sample Information . . . 23
- 6.2 Hydrogen Plasma Source and Conditions . . . 23
- 6.3 Hydrogen Plasma Exposures . . . 24
  - 6.3.1 PL . . . 24
  - 6.3.2 XRD rocking curves . . . 26

6.4 Annealing . . . 26
6.5 Conclusion . . . 27
6.6 Outlook . . . 28

7 XSTM study of hydrogen passivated N:GaAs 29
7.1 Observed Features . . . 29
7.1.1 Feature A . . . 32
7.1.2 Feature B . . . 32
7.1.3 Feature C . . . 33
7.2 Feature Related Observations . . . 35
7.2.1 Filled State Imaging . . . 35
7.2.2 Empty State Imaging . . . 36
7.3 General Observations on Hydrogen Passivated N:GaAs . . . 37
7.4 Possible Lattice Orientations of the Observed Features . . . 38
7.4.1 Feature A . . . 38
7.4.2 Feature B . . . 38
7.4.3 Feature C . . . 40
7.5 Conclusion . . . 40
7.6 Outlook . . . 41

8 Conclusions and Outlook 42

Bibliography 45

Chapter 1

Motivation

Modern society relies heavily on computing power, not only for our personal computers and mobile phones but also in data centers and supercomputers supplying us with all the information we want. In recent years the computing power of a single chip has reached its limits due to power dissipation issues. The heat created in the chip cannot be removed efficiently enough to operate at higher frequencies. To circumvent this limit parallel computing has took off in a major way. At the on-chip level, by putting more cores on a chip, and on a larger level by linking multiple computers. This requires fast, but also low-power, communication between the parallel parts to ensure information can be shared between all parts [1].

One solution currently being researched is the integration of low-power optical components on chip. If the data created on the chip can be converted to an optical signal, transported to the other chips in the systems and converted to an electrical signal again, this could be an fast method of communication. This requires a collection of optical components to be implemented on, or very close to, the chips. This includes single-photon emitters, waveguides and detectors.

Semiconductor quantum dots (QDs) have shown to be a good single photon sources [2], whose spatial and spectral properties can be controlled [3]. This control is required for efficient coupling of the emitted photons into waveguides and other components; a small displacement of the QD can lead to a strong decrease in coupling efficiency [4]. There are multiple techniques used for growing QDs. With strained layer (Stransky-Krastanov) growth material choice is limited due to the required lattice mismatch and overgrowing the QDs can cause them to deform or dissolve [5] [6]. Growth by droplet epitaxy allows for a more free choice in materials but still suffers from inhomogeneity in the shape of the QDs [7]. Both techniques offer no control over the position of the QDs without additional sample preparation techniques [8].

A new method of creating QDs was discovered recently and is already showing promising results in terms of single photon emission [9]. Introduction of a few percent of N in GaAs causes a strong decrease of the bandgap and an appearance of tensile strain in the material. By controlling the concentration of N the spectral properties of the material can be tuned. Exposing grown N:GaAs to hydrogen ions restores the bandgap to the N free material and can convert the strain from tensile to compressive. This has been attributed to the formation of NH complexes, which neutralize the effects of nitrogen. This passivation is stable up to a temperature of 250C. Above this temperature the thermal energy will start to reverse the passivation process, and after a few hours restoring the as-grown properties of the material [10]. An even more interesting discovery is that the passivation can also be undone by light irradiation, which opens up the possibilities of controlling the passivation at a local level.

With the use of local laser treatment [11] [12] or scanning near-field optical microscope irradiation [9] nanostructures can be created. Another way to create these structures employs the fact that the hydrogen passivation shows a sharp front. By depositing a hydrogen-opaque mask with the desired structure on the sample before passivation, the material under the mask will not be passivated [13]. These techniques can be used to create QDs with precise control over their location and size.

The exact nature and shape of the NH-complexes formed after hydrogen passivation has been a subject of extensive studies. Most research done on this topic employed techniques to indirectly observe the complexes, with no direct studies at the atomic level. Our group has a long history in real space single dopant observation and manipulation, in particular iso-electronic impurities [14] [15]. N:GaAs has been studied in detail in our group [16] [17], which should provide a strong foundation to expand to hydrogen passivated N:GaAs. In this research we will try to perform the hydrogen passivation using tools available at the TU/e and check the results of this using photoluminescence and X-ray diffraction rocking curve measurements. We will then continue with the direct visualization of the formed NH-complexes using cross-sectional scanning tunneling microscopy and also try to locally remove the hydrogen from these complexes using the STM. Since we can directly study the NH-complexes this should hopefully provide more information on their exact shape and orientation in the GaAs crystal lattice.

Chapter 2

Introduction

2.1 Iso-electronic Impurities

Traditional semiconductor doping introduces atoms with one valence electron more, or less than the atom it replaces. In this way extra electrons or holes are introduced into the material, tuning the Fermi level. It is also possible for an atom to be replaced with one with the same number of valence electrons. Such substitutions, with elements of the same group, are called iso-electronic impurities. Iso-electronic impurities introduce no new carriers in the host material, since they replace an atom with the same number of valence electrons. Examples of iso-electronic impurities are nitrogen (N) and bismuth (Bi) in GaAs. Both will replace an arsenic (As) atom in the lattice, causing a local deformation of the lattice and a redistribution of the electrons around them because of the difference in electronegativity. In the case of N the lattice will locally be pulled towards the N atom because it is smaller than the As atom it replaced. In the case of the, bigger, Bi the atoms around it are pushed outwards.

The iso-electronic impurities do not dope the host material in the traditional way, but they can still influence the electronic properties. Taking the example of N in GaAs, one might expect that the bandgap of N:GaAs linearly shifts from the intrinsic GaAs one to the, more than twice as large, bandgap of GaN [18]. Instead with small concentrations of N the bandgap of the N:GaAs becomes smaller than the one of GaAs [19] [20] [21]. Similar effects have been observed in many different III-V semiconductor alloys, including GaAsBi [22], InAsN [23], InAsBi [24]. These materials are also called highly mismatched alloys (HMAs) since the ternary element introduced has a significantly different size then the original element.

The model describing the strong band bowing observed in these HMAs is the band anti-crossing model (BAC). If a highly electronegative atom replaces a anion in a semiconductor material this will introduce a localized state near the conduction band edge [25] [20]. This state interacts with the extended states of the host material causing the conduction band to split into a E+ and E- band and thus reducing the size of the bandgap as illustrated in Figure 2.1 [26].

For large-sized impurity atoms with a first ionization energy lower than the original anion, the impurity state introduced by the atom lies usually close to the valence band. In this case the impurity states cause the light hole (LH), heavy hole (HH), and spin-orbit split-off band to restructure in E+ and E- bands according to the valence band anti-crossing (VBAC) model. The anti-crossing interaction between these split-off E+ and E- bands causes the E+ band to move up in energy, reducing the size of the bandgap [27].

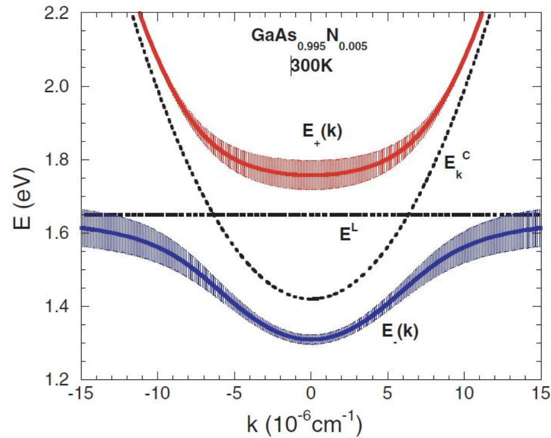

Figure 2.1: Schematic showing the effect of the Band Anti-crossing in N:GaAs. Adapted from Ref [26]

2.2 Hydrogen Passivation in Semiconductors

Incorporation of atomic hydrogen in general semiconductor materials has a significant impact on their optical and electrical properties. Hydrogen passivates the electronic activity of dangling bonds and can also passivate shallow donor and acceptor impurities in compound semiconductors [28] [29]. Hydrogen passivation is applied in production processes for the neutralization of defects in silicon wafers [30] [31].

It also has a major effect in GaPN, where it causes a restoration of the bandgap energy towards the value of intrinsic GaP[32] [33]. In GaAsBi it neutralizes shallow acceptor states, and increases the hole mobility tenfold, but does not restore the bandgap energy [34] [35]. InAsN shows no restoration of the bandgap energy either [36].

2.3 Effects of Hydrogen Passivation on N:GaAs

The first observed effect of hydrogen on dilute nitride semiconductors was seen in Refs [38] [39], where the bandgap of the material was restored towards the N free alloy. Here, the grown material was exposed to a flux of atomic hydrogen originating from a Kaufman plasma source [40]. The effect of hydrogen passivation on the bandgap is visible in photoluminescence (PL) spectra by a shift in the spectral weight from the N induced peak back to intrinsic GaAs with increasing H dose [41]. Another effect observed was conversion of the tensile strain in the as-grown material, to compressive strain after hydrogen passivation, which was measured using X-ray diffraction (XRD) rocking curves [42]. During the passivation treatment the hydrogen diffuses through the material with a very sharp front, where the decay length of the hydrogen concentration can be as short as 5 nm/decade depending on the temperature of the sample [40]. The distance between pairs of nitrogen atoms influences their rate of passivation [32] [37]. It has been shown that hydrogen binds more effectively to closer spaced pairs, resulting in a shift in the spectral weight with the peaks corresponding to single N atoms becoming more important.

Following the discovery of the hydrogen passivation in N:GaAs, research started to discover the exact nature of the hydrogen complex. An early density functional theory (DFT) study proposed a N-H_2^* complex [43]. Vibrational spectroscopy showed results that did not reconcile with the properties of the N-H_2^* complex, suggesting that another complex is involved [44]. This theory was strengthened by an X-ray absorption study, also showing no evidence of the N-H_2^*-complex. In addition, this paper suggested another possible complex, C_{2v} [45]. Later studies confirmed the existence of the C_{2v} symmetry complex [46] and its canted variant, the C_{1h} complex [47] [48]. A

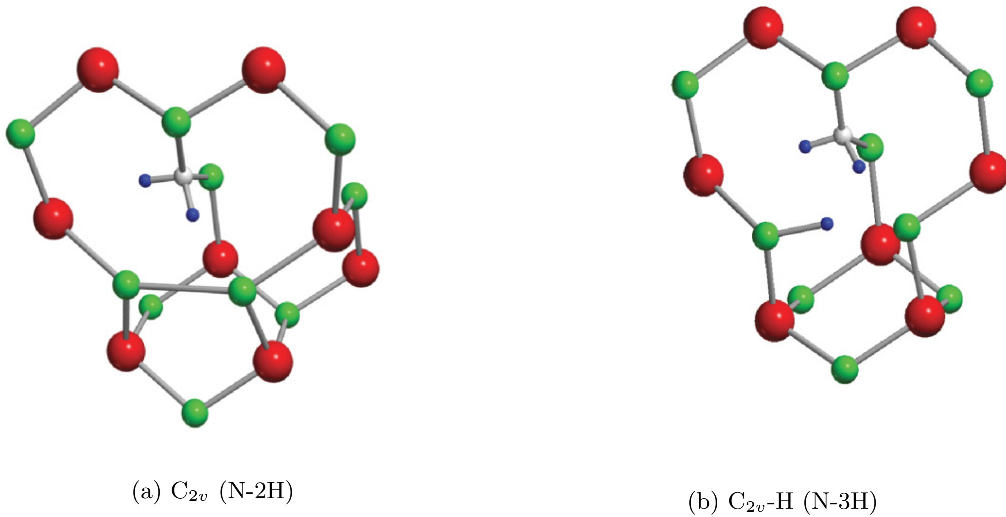

(a) C_{2v} (N-2H)

(b) C_{2v}-H (N-3H)

Figure 2.2: Schematic view of the N-2H and the N-3H complexes with the Ga, As, N, and H atoms colored green, red, white, and blue respectively. Adapted from Ref [37]

more recent paper followed in 2014 by Amidani *et al* [49]. In GaAsN the N atom binds to its Ga neighbors in a symmetric fashion. With the formation of the H complex two of these N-Ga bonds are broken, binding two H atoms to the N atom. This allows the N atom to displace towards the Ga atoms it is still bound to, which in turn also relax to their original position in the lattice. The other two Ga atoms can both bind a H atom, forming the C_{2v}-H or C_{2v}-2H complex as displayed in Figure 2.2 [49]. For convenience sake the C_{2v} and C_{2v}-H symmetry complexes will be referred to as N-2H and N-3H respectively.

The N-2H complex removes the tensile strain introduced by the N and passivates the electronic activity of nitrogen, returning the bandgap to that of intrinsic GaAs. The N-3H complex introduces compressive strain in the lattice, but does not influence the bandgap. Through thermal annealing the two complexes can selectively be removed. At 250°C the N-3H complex starts to dissolve, removing the compressive strain. At 330°C, when the N-2H complex disassociates, the strain returns to tensile and the bandgap is restored to the as-grown N:GaAs [50].

2.4 Functional Passivation

As discussed in Section 2.3 NH-complexes can be disassociated using thermal annealing, restoring the properties of material before passivation. Unfortunately this does not allow for control of the passivation of the nitrogen at a local level. The first papers mentioning local control of the passivation of N in GaAs appeared in 2011, with one employing spatially selective passivation [51] and the other using local removal of hydrogen through the use of a high-intensity laser [11]. The spatially selective passivation was realized by depositing a hydrogen-opaque Ti mask on the surface of the sample as illustrated in Figure 2.3. The combination of the sharp hydrogen front during passivation and a well controlled exposure time allows for the creation QDs. The spatial control over the placing of the QDs is limited by the resolution of the Ti deposition technique. The *size* of the QD is not limited by this, as shorter or longer hydrogen exposure times are used to control the size.

The laser-assisted removal has been attributed to photon-assisted disassociation of the complex, though the exact mechanisms of the process are still unknown [11] [12]. Local removal has been recently expanded to scanning near-field optical microscope irradiation (SNOM), realizing higher positional accuracy [9].

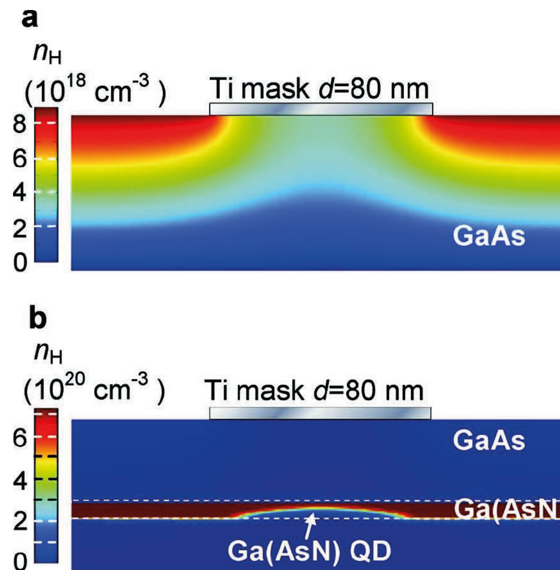

Figure 2.3: Area selective passivation of GaAs (a) and a GaAs/N:GaAs QW (b)

Chapter 3

Theory

3.1 Scanning Tunneling Microscopy

After the invention of the scanning tunneling microscope by Binning and Rohrer in 1981 [52], it developed quickly into an important technique for studying surfaces of metals and semiconductors at the atomic scale. Scanning tunneling microscopy (STM) is a scanning probe technique which relies on the tunneling current between an atomically sharp tip and a conducting sample. The tip is controlled with piezo-actuators for fine control. This allows the tip to come close enough to the sample surface that electrons can tunnel from the tip to the sample when a bias voltage is applied. A schematic representation of an STM is given in Figure 3.1.

At its core STM has two measuring modes, constant current and constant height. During constant current mode the height of the tip is controlled by a feedback loop, keeping the current constant. The bandwidth of the feedback loop limits the scan speed in this mode. In constant height mode the height of the tip is not changed and the changes in current are measured to provide information on the sample. This allows faster scanning because the feedback loop is turned off, but creates a greater risk of collisions between tip and sample, and potentially destroying the tip. For this reason all images are made in constant current mode.

A clean, flat surface is important for STM measurements, which can, in an ideal world, be achieved by thorough cleaning of the surface to remove oxides and other contaminants. When this is done on a wafer with grown epilayers, it would still only allow us to measure the last grown layer, since STM is a surface technique. A way around this is to employ a special sample preparation method and perform cross-sectional STM (XSTM). This is achieved by cleaving the sample under ultra-high vacuum conditions along the non-polar (110) planes, revealing an atomically flat cross-section of the sample. The vacuum conditions will ensure that the highly-reactive dangling bonds revealed after cleaving are not immediately reacting with the atmosphere.

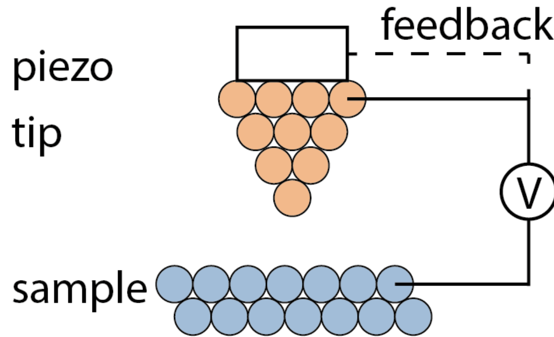

Figure 3.1: Schematic image of the basic components of an STM: a tip controlled with piezo-actuators, a conducting sample and a feedback loop to control the tip.

3.2 DOS and LDOS of Semiconductors

To better understand the interaction between the tip and the sample, this section will go into more detail about conductivity at a solid state level. The density of states (DOS) $\rho(E)$ of a material describes the number of states present at a certain energy range and can be written as

$$dN(E, E + dE) = \rho(E)dE, \tag{3.1}$$

for the case of an energy range between E and $E + dE$. Taking a finite energy range, E_1 to E_2, the number of states becomes

$$N(E_1, E_2) = \int_{E_1}^{E_2} \rho(E)dE. \tag{3.2}$$

If the system has n discrete energy states the DOS can now be written as

$$\rho(E) = \sum_n \delta(E - E_n), \tag{3.3}$$

where δ is the Dirac delta function.

For the purposes of STM a quantity related to the DOS is also important, the local density of states (LDOS), which gives the DOS at a specific location $\mathbf{r}$. The expression for the LDOS is

$$\rho(E, \mathbf{r}) = \sum_n |\phi_n(\mathbf{r})|^2 \delta(E - E_n). \tag{3.4}$$

3.3 Tunneling Theory for STM

Bardeen developed a model for tunneling in metal-oxide-metal junctions [53], which considers the tunneling conditions for the metal-oxide and oxide-metal interface separately. Applied to the subject of STM these will be a tip-vacuum and vacuum-sample transition respectively. The transition probability from the tip state to the sample state is described by time-dependent perturbation theory.

A schematic overview of the system is given in Figure 3.2, where tip and sample are metallic with work function Φ. The Fermi energy of the tip and the sample are $E_{F,t}$ and $E_{F,s}$ respectively. Here a negative bias V is applied between tip and sample. Assuming the zero temperature limit, all states up to the Fermi level are occupied, and all states above are empty. As a result transitions can only take place for states in the energy range between $E_{F,t}$ and $E_{F,s}$.

For this situation Bardeen derived the following expression for the tunnel current

$$I = \frac{4\pi e}{\hbar} \sum_{i,f} |M_{fi}|^2 \delta(E_f - E_i), \tag{3.5}$$

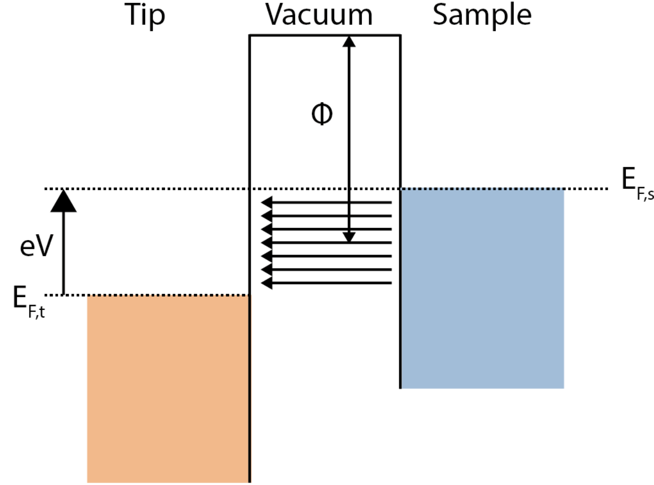

Figure 3.2: Schematic image of the tip-vacuum-sample tunnel junction at negative bias voltage V. Both tip and sample are assumed to be metallic with a work function Φ. Colored parts indicate filled states. Horizontal arrows in the gap indicate from which states and in which direction tunneling can take place.

where e is the electron charge, M is the matrix element of the tunneling probability, and E_i and E_f are the initial and final state respectively. The Dirac delta indicates that tunneling can only happen for states with the same energy. The most challenging part of the Bardeen model is calculating the tunneling matrix elements, as these depend on the energy. To simplify this problem, Tersoff and Hamann made an approximation of the Bardeen theory assuming there is no energy dependence of the matrix element and evaluating it at small voltages [54]. As a result of these approximations it is assumed that the major contribution to the tunneling current comes from states very close the Fermi level. To now calculate the tunneling matrix element explicit wave functions for the sample surface and tip are defined. The sample is described by a plane wave Fourier expansion, while the tip is approximated in its simplest form, by a point source having an s-like wave function. The expression for the tunneling current then reduces to

$$I \propto \sum_n |\psi_n(r_t)|^2 \delta(E_n - E_F), \tag{3.6}$$

which is the expression for the local density of states of the surface, as seen before in Section 3.2. As a result an ideal STM experiment only measures the LDOS of the sample. The approximation holds for tips with a finite size, as long as the tip wave function can described by an s-orbital.

Here the barrier was assumed to be rectangular. If we now take into account that tip and sample can have a different work function, the barrier will have a trapezoidal shape. The average barrier height is then given by the average of the two work functions

$$\bar{\Phi} = \frac{\Phi_t + \Phi_s}{2}, \tag{3.7}$$

where Φ_t and Φ_s are the work functions of the tip and sample respectively. Also taking into account the applied bias and the tunneling energy ϵ gives the effective barrier height

$$\Phi_{eff} = \frac{\Phi_t + \Phi_s}{2} + \frac{eV}{2} - \epsilon. \tag{3.8}$$

The transmission factor is now given by

$$T(\epsilon, V, d) \propto exp\left(-d\sqrt{\frac{2m}{\hbar^2}\left(\frac{\Phi_t + \Phi_s}{2} + \frac{eV}{2} - \epsilon\right)}\right). \tag{3.9}$$

3.4 Topographic and Electronic Contrast in STM

STM can measure the topography of a sample and also its electronic properties, it actually measures both at the same time. Consider, for example, an area that is higher than its surroundings; the tip will be closer to the surface and as a result the tunnel current will increase. To counteract this the feedback loop will move the tip up to keep a constant tunnel current. If instead the tip encounters an area with a higher conductivity (at the applied bias voltage) the tunnel current will also increase and cause the tip to move up. So a region which is physically higher and a region that has a higher conductivity can look the same in an STM measurement.

By measuring at specific voltages the cross-talk between the two contrasts can be reduced. For example, N atoms in GaAs influence the states around the conduction band. By measuring at negative voltages (pulling electrons from the valence band) the electronic effects of N are almost not measured. Instead we can observe the structural effects N atoms have on the lattice.

Usually electronic features are highly dependent on the bias voltage, so by measuring the same area at different voltages you can try to get insight if features have electronic or topographic origins.

3.5 STM on (110) surfaces

The (110) surface of a zinc-blende semiconductor consists of zig-zag rows along the [110] or $[1\bar{1}0]$ direction, which contain an alternating pattern of anions and cations, as shown schematically in Figure 3.3(b). In the [001] direction the distance between atoms of the same type is equal to the lattice constant a, while in the $[110]/[1\bar{1}0]$ direction the distance is $a/\sqrt{2}$.

All atoms at the cleaved surface have one dangling bond, which gives rise to an anionic A_5 and a cationic C_3 surface band, which are located within the bandgap. The A_5 state has a lower energy than the C_3 state [55]. The surface undergoes a buckling where the anions move outwards and the cations move inwards by means of a buckling of the bonds [56] [57] as displayed in Figure 3.3. This relaxations causes a redistribution of charge in the surface atoms, filling the dangling bond of the anions with an electron and leaving the cation dangling bond empty [58]. Another effect of the buckling is that the A_5 and C_3 state are pushed out of the bandgap into the valence band and conduction band respectively as illustrated in Figure 3.4(a).

In addition to the A_5 and C_3 state, two other states play a role in the interpretation of STM images of the (110) surface, the A_4 and C_4 state. The A_4 and A_5 are located mainly on the group V atoms at the surface, while the C_3 and C_4 states are concentrated at the group III atoms. At negative tunneling voltages electrons are pulled from the filled states in the valence band, while at positive voltages electrons are injected into empty states in the valence band. This allows for the selective imaging of the anionic or cationic states by choosing the right bias voltage and can

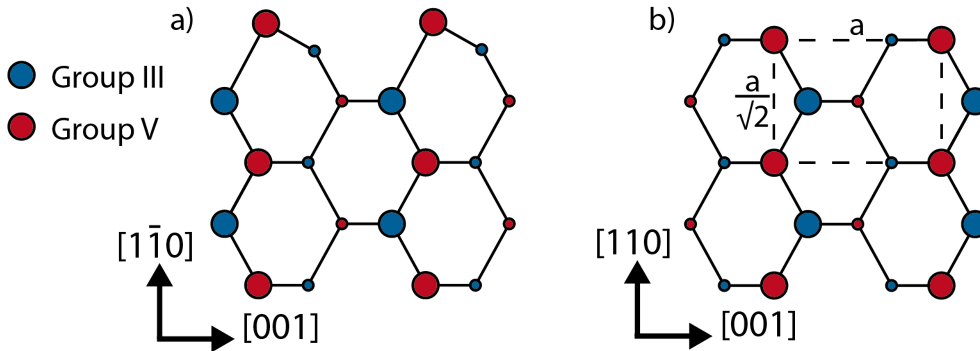

Figure 3.3: Schematic overview of the cleaved (110) surface, with the group III and V elements colored blue and red respectively. (a) shows a relaxed side view of this surface, while (b) shows the top view. In (b) a marks the lattice constant.

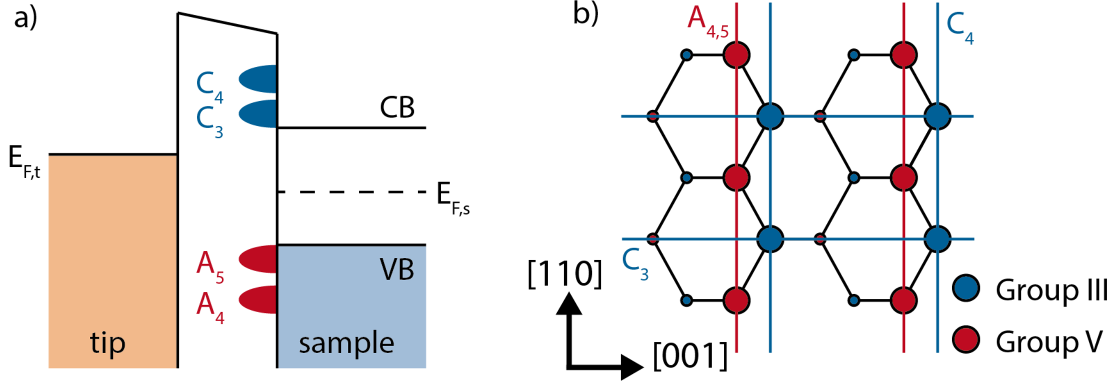

Figure 3.4: Energetic and spatial distribution of the cationic $C_{3,4}$ and anionic $A_{3,4}$ surface states of the (110) plane. (a) shows a schematic band diagram of the tip and the sample after the reconstruction of the surface, with the surface states outside of the bandgap. (b) shows the spatial distribution of the cationic $C_{3,4}$ and anionic $A_{3,4}$ surface states

be used to determine the orientation of the crystal lattice. By changing the polarity of the bias voltage halfway through a measurement a shift of the corrugation of $0.25a$ can be observed.

Another important difference between the A and C states is their orientation, the A_4, A_5 and C_4 states extend along the zigzag rows, while the C_3 state extends perpendicular to them, as illustrated in Figure 3.4(b). With this some insight can be gained in which bias voltages addresses which energy levels.

3.6 XSTM on N:GaAs

Nitrogen atoms in a cleaved (110) surface of N:GaAs have been identified as depressions of the surface under filled state imaging conditions [59] [60] [16]. Defining the surface layer as layer 1, N atoms in odd layers show a depression on a single anion site, while N in even layers shows as a depression on four anion sites. The layer below the (110) surface in which the atoms reside is determined by the depth of the observed features. N atoms deeper below the surface cause less distortion and as a result show a weaker contrast. An overview of these features is given in Figure 3.5(a).

DFT calculations were employed to compute the atomic and electronic structure of the (110) GaAs surface with N centers in different layers below the surface. From this simulated XSTM images were made for comparison with actual measurements and for N:GaAs the images were found to be in good agreement [14]. In general the covalent radius of the iso-electronic impurities was found to play a major role in interpreting the structural effect the atoms have on the (110) surface. The covalent radius is the effective size of an atom when it is covalently bonded to other atoms.

At empty state imaging conditions the N atoms show a bright contrast and have a strong dependence on the applied bias voltage [61] [17]. These cross-like features have a strong anisotropy between the [001] and [110] direction. For deeper N atoms the bright contrast spatially extends further, but is generally less intense. These results were also compared with tight-binding simulations and were found to be in good agreement as displayed in Figure 3.5(b) and (c).

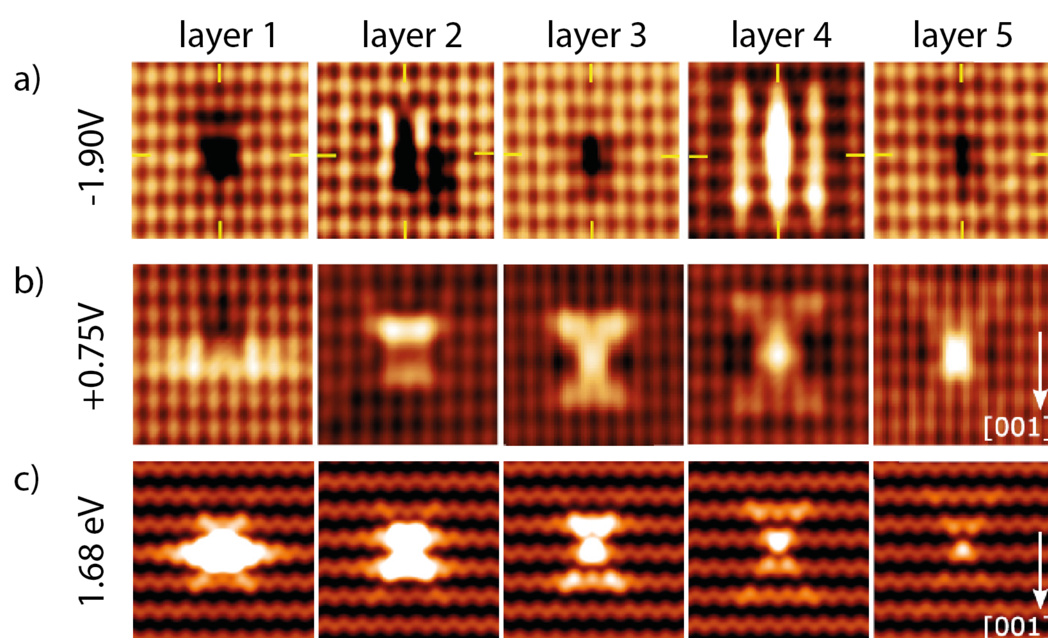

Figure 3.5: Filled (a) and empty (b) state images of N atoms in different layers below the (110) surface. (c) displays tight binding simulations at the energy of the empty state images (b). Layer 1 corresponds to an N atom in the surface plane. Adapted from Ref [17]

Chapter 4

Experimental Methods

4.1 Tip Induced Band Bending

For interpretation of STM results it is important to consider the effect of the tip on the band structure of the sample. Metals will shield the electric field of the tip very effectively due to high amount of free carriers available. The same goes for semiconductors with a pinned Fermi level at the surface caused by surface states. For semiconductors with an unpinned Fermi level at the surface the electric field of the tip will penetrate deep into the sample, leading to a bending of the energy bands of the material. Before the tip and sample are brought into (tunnel) contact they have flat bands and different work functions, Φ_t and Φ_s respectively. The work function is the energy difference between the Fermi level and vacuum level of a material. For a semiconductor the work function is given by $\Phi_s = \chi + E_g - E_F$, where χ is the electron affinity, E_g is the bandgap and E_F is the Fermi level. From this expression it can be seen that the work function of a semiconductor can be tuned by controlling the doping and in turn, the Fermi level.

When tip and sample are brought into (tunnel) contact the system will find an equilibrium, with equal Fermi levels for tip and sample. To achieve this equilibrium the bands of the sample will bend, which is called tip induced band bending (TIBB). A schematic overview of the effects of TIBB on an n-doped sample is displayed in Figure 4.1. When a negative bias voltage is applied between tip and sample the bands are bent downwards near the surface. Since the states in the tunnel window lie below the Fermi level, this mode is called filled-state imaging. If a positive bias is applied instead, the band will bend upwards, pulling states above the Fermi level into the tunneling window, and the measuring condition is called empty-state imaging.

The work function of the tip is very much dependent on its shape and size, and can change over the course of a measurement, making it difficult to obtain a value for the TIBB [62].

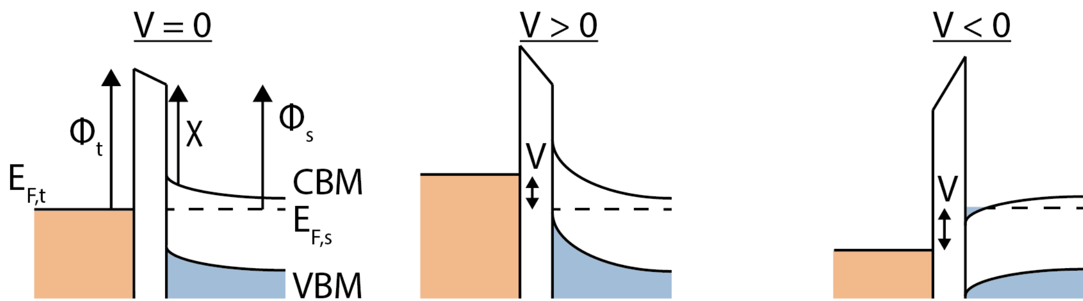

Figure 4.1: Schematic image of the effects of tip induced band bending in an n-doped sample with an applied bias V, where $E_{F,t}$ and $E_{F,s}$ are the Fermi level of the tip and sample respectively, CBM is the conduction band minimum, VBM is the valence band maximum, χ is the electron affinity, and ϕ_t and ϕ_s are the work functions of the tip and sample respectively.

4.2 Scanning Tunneling Spectroscopy

Scanning tunneling spectroscopy (STS) is used to study the dependence of the tunneling current on the applied bias voltage. The following describes the experimental method of performing STS. First the tip is kept stationary above a certain point of the sample until the tunnel current stabilizes. The feedback loop is then switched off and slow sweep of the bias voltage is performed while measuring the tunnel current, in this way a I/V curve is recorded. If desired, the tip is brought closer to the surface after the stabilization, in this way the obtained signal can be increased.

While I/V curves are interesting, the derivative, dI/dV, curves are usually of greater value, since they represent the density of states of the sample. An expression for dI/dV can be obtained by evaluating the equation for the tunnel current

$$I = \frac{4\pi e}{\hbar} \int_0^{eV} \rho_t(\epsilon - eV)\rho_s(\epsilon)T(\epsilon, V, d)d\epsilon, \tag{4.1}$$

at the upper limit $\epsilon = eV$, where ρ_t and ρ_s are the DOS of tip and sample respectively, and $T(\epsilon, V, d)$ refers to the transmission factor between tip and sample. This gives

$$\frac{dI}{dV} \approx \frac{4\pi e}{\hbar}\rho_t(0)\rho_s(eV)T(eV, V, d). \tag{4.2}$$

If we assume, as a further approximation that the DOS of the tip and the transmission factor are independent of the voltage, the equation reduces to

$$\frac{dI}{dV} \propto \rho_s(eV), \tag{4.3}$$

so in approximation STS measures the DOS of the sample.

dI/dV curves can be obtained from recorded I/V curves through numerical differentiation, but these derived curves often suffer from poor signal to noise ratio. dI/dV curves can also directly be obtained by applying a lock-in technique to the spectroscopy measurements. By adding a modulating sinusoidal voltage to the bias voltage, the signal can be detected by a lock-in amplifier. By using longer averaging times for the lock-in detection the signal to noise ratio can be improved, but in practice the averaging time is limited by the drift of the piezo elements. If the averaging takes too long the tip will drift and change its distance to the sample and as such changing the tunnel current.

The transmission factor, as given by Equation 3.9, contains the effective barrier height. As a result, states with a smaller tunnel barrier have a higher transmission probability, and as such contribute more to the tunnel current. With the increasing bias voltage V during a STS measurement the transmission factor increases even further causing a exponential increase of the tunneling current, which starts to dominate the dI/dV signal. A way to remove this voltage dependence was shown in Ref [63]. Here the dI/dV curve is normalized with the measured I/V. Unfortunately this poses a problem when performing STS on semiconductors. If the bandgap of the semiconductor lies within the measured voltage range both the differential conductance and normal conductance may go to zero leading to divergence of the signal.

Another important thing to keep in mind is that STS measurements also contain information about the DOS of the tip. To ensure the measurements are not influenced too much by the tip DOS they should ideally be repeated with a different tip.

4.3 STM Setup

The STM system used for the experiments in this report is a commercial Omicron LT-STM, of which a schematic overview is displayed in Figure 4.2. The whole setup is located on an actively damped table in an acoustically isolated chamber. The floor of this chamber is decoupled from the rest of the building providing further mechanical stability. The system consists of a three

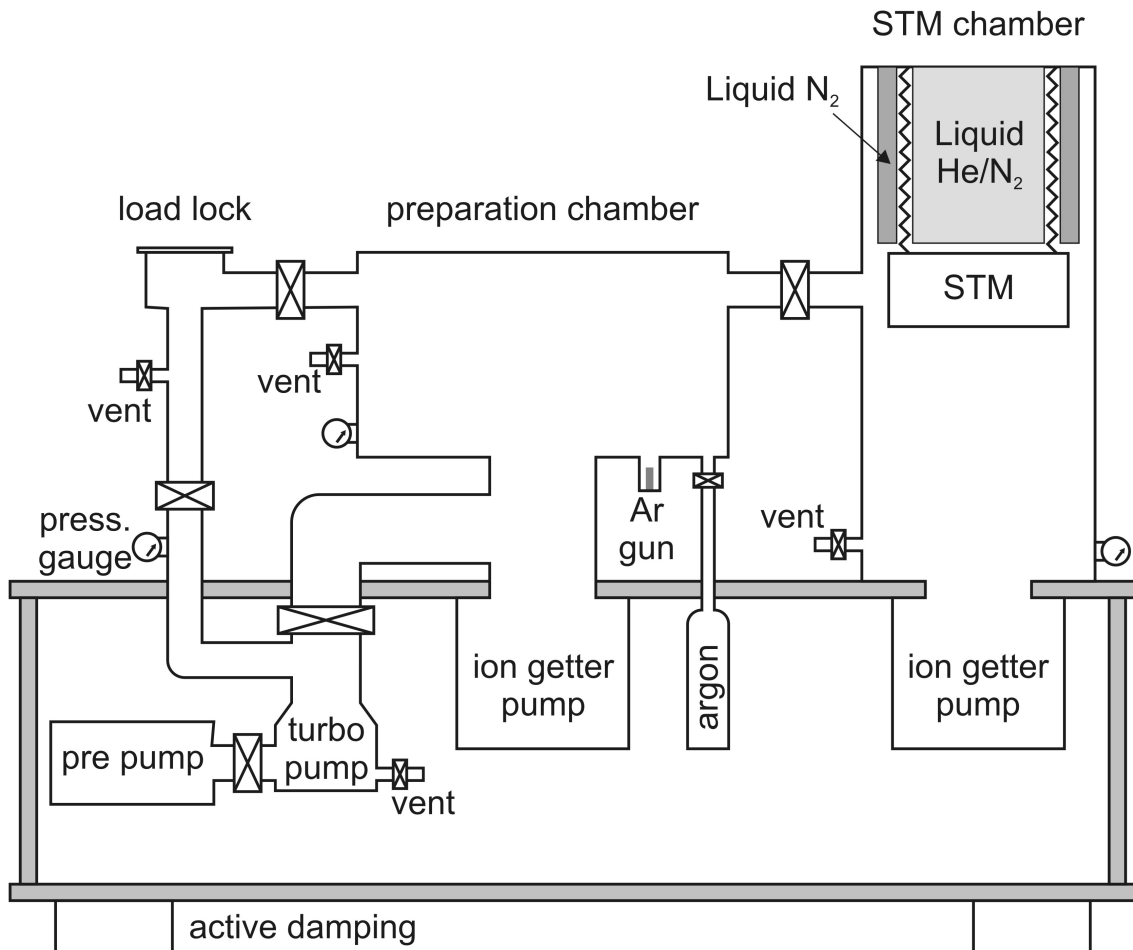

Figure 4.2: Schematic overview of the Low Temperature - Scanning Tunneling Microscope setup, adopted from Ref [64].

of vacuum chambers connected via transfer tubes, which can be closed off using gate valves. A load lock, pumped by a turbomolecular pump in series with a scroll pump, is used to transfer samples and tips in and out of the system. The load lock connects to a preparation chamber, which contains a contact-resistance heater and an ion gun for *in-situ* treatment of samples and tips. The heater is used to clean samples and tips of organic matter and water, while the ion gun is used to sputter tips with argon to remove oxide. Under normal circumstances the preparation chamber is pumped using an ion getter pump, but during baking and sputtering it is pumped using the turbomolecular pump to prevent contamination of the ion getter pump.

The STM chamber contains locations for sample and tip storage and the main STM construction. The STM is surrounded by two concentric cryogenic shields, which are connected to two separate baths. The outer bath, connected to the outer shield, can be filled with liquid nitrogen (LN_2), while the inner bath can be filled with either LN_2 or liquid helium (LHe) to cool the STM to 77K or 4K respectively. Measuring at LHe temperature provides greater thermal stability and reduced piezo drift, important for long measurements such as STS. The downside of measuring at LHe temperature is the reduced conductivity of the sample. When cooling down the STM is pressed against the inner cryostat bath to provide the best thermal contact. During measurements the STM is decoupled from the cryostat using a set of springs, providing even greater vibrational stability. To reduce vibrations, the turbomolecular pump and scroll pump are turned off during measurements.

The vacuum in the preparation chamber is maintained at $1 \cdot 10^{-9}$ mbar, while the vacuum in the STM chamber is kept below $5 \cdot 10^{-11}$ mbar.

4.4 Sample Preparation

Samples are created by breaking out a 4 by 8 mm rectangle of material from a wafer. To ensure a good electrical connection between the sample and the sample holder, contacts are deposited on the sample using thermal evaporation. For n-doped samples the contact consists of germanium (Ge), nickel (Ni), and gold (Au). Ge is used to ensure an Ohmic contact because its work function is very close to that of GaAs, Ni is used as a buffer layer, and Au provides a good electrical contact to the sample holder.

It is essential that cleaving the sample creates a surface that is as close to atomically flat as possible. To ensure this, as-grown samples are mechanically polished to reduce their thickness to around 150 to 120 μm. This thickness strikes a balance between providing a good cleave and ensuring that the sample does not unintentionally cleave during the remaining preparation steps. A scratch of about 1 mm long is made on the sample to control the location of the cleave. The sample is then clamped in a sample holder, with small slices of indium on both sides. The sample holder is heated up, melting the indium slices to provide good electrical contact between the sample and the sample holder.

After moving the samples into the STM system, they are baked at 180°C for 25 min to clean them. Samples are cleaved in the UHV environment of the STM chamber to avoid contamination of the cleaved surface. By cooling the sample down to 77K immediately after cleaving, the revealed surface can be kept clean for more than two weeks.

4.5 Tip Preparation

Tips are created by chemically etching poly-crystalline tungsten (W) wire. A 17 mm long piece of wire is cut off, attached to a tip carrier and suspended in a 2 M potassium hydroxide (KOH) solution. The wire acts as the first electrode for the etching process, a platinum counter-electrode also suspended in the KOH solution completes the circuit. By applying a voltage between the electrodes the chemical etching process is started. This etching is comprised of the following redox reaction

$$W(s) + 2\ OH^-(aq) + 2\ H_2O(l) \rightarrow WO_4^{2-} + 3\ H_2(g). \quad (4.4)$$

The etching takes place primarily at the meniscus where the wire enters the solution, because products of the reaction (WO_4^{2-}) fall down along the wire and cover the bottom, preventing further etching. After some time the part of the wire below the meniscus falls off, creating a tip. After transferring them to the STM system, the tips are baked for 30 minutes at 230°C with the contact-resistance heater in the preparation chamber and then sputtered with argon (Ar) to remove oxides and ensure tip sharpness.

If the tip does not provide the desired resolution during measurements, voltage pulses can be applied to it, to try and change the shape of the tip apex.

4.6 Other Measurement Setups

4.6.1 Photoluminescence

PL measurements at the TU/e were all performed at low-temperature (10 K). Excitation was achieved with a 635 nm continuous-wave laser and PL signal was collected using a spectrometer and a LN_2 cooled CCD.

4.6.2 X-ray Diffraction

X-ray diffraction (XRD) relies on two basic components, an x-ray source and a detector. X-rays scatter off a sample and are collected at the detector. For XRD rocking curves (XRD-RCs) the source and detector are kept stationary while the tilt of the sample is changed. The intensity of the x-rays at the detector is now recorded as a function of the tilt angle. For samples with grown layers, these measurements will usually show a peak caused by the substrate, one peak from the grown layer(s), and oscillations in the intensity caused by the thickness of the layer (fringes). XRD-RCs were obtained using a Panalytical X′Pert Pro X-ray diffractometer.

Chapter 5

Sample preparation and characterization

This chapter provides information on the hydrogen passivation of the samples used in the STM measurements. First, the structure of the different samples is provided. Then the passivation conditions and simulations of the passivation process are discussed. And lastly, the PL spectra obtained from the samples before and after the passivation are compared and discussed to support that the passivation of the samples was successful.

Hydrogen passivation of the samples was done by Mayank Shekhar Sharma and Marco Felici at Sapienza University of Rome. They also performed the simulations of the passivation process and measured the PL of the samples.

5.1 Samples

STM measurements were performed on two different samples. These samples were grown with MBE by Alicia Gonzalo in the group of Jose Maria Ulloa at the Institute for Optoelectronic Systems and Microtechnology of the Universidad Politécnica Madrid.

Sample 2131 has a GaAs Si-doped substrate, 250 nm of undoped GaAs buffer layer and 200 nm of N:GaAs with a N concentration of 0.62%.

Sample 2233 has a more complicated structure, with multiple QWs. This design was chosen to have layers with multiple N concentrations in one sample and to have passivated and non-passivated layers so they can be compared. A schematic overview of its sample design in displayed in Figure 5.1. On the right side of this figure is the Si-doped GaAs substrate on which the layers are grown. Going from right to left, first a GaAs buffer layer is grown, then the first set of three QWs and a 100 nm layer with an N concentration of 1%. After this, another set of three QWs and on top of this a Si-doped GaAs capping layer. The numbers on the top of the image indicate the different N:GaAs QWs. The N concentrations of QW 1, 2 and 3 are 0.85 %, 0.53 % and 0.35% respectively. The N concentrations of QW 4, 5 and 6 are again 0.85 %, 0.53 % and 0.35% respectively. The numbers in the layers indicate their thickness, while the colors indicate the material. The top half of the structure, from QW 1 to QW 3, is passivated with hydrogen post-growth as indicated by the blue bar at the bottom.

The 1% N layer in the middle of the grown structure was build in to ensure that QW 4 to 6 are not passivated. While the diffusion of hydrogen usually shows a very sharp front, any stray hydrogen should be caught in this layer before it reaches the lower QWs.

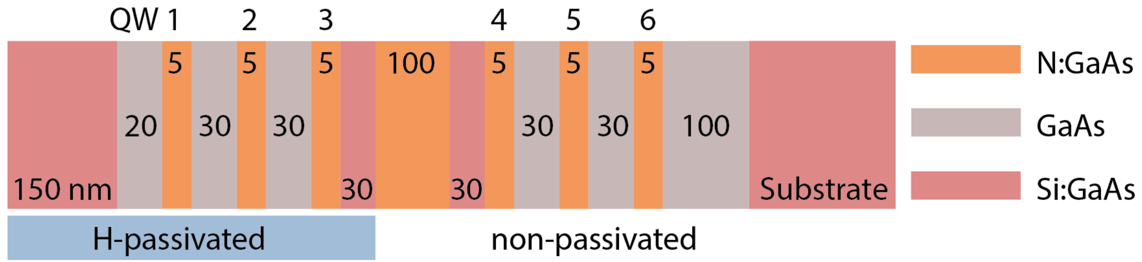

Figure 5.1: Sample design of 2233, where the substrate on which the layers are grown in located on the right of the image. Layers are grown on top of this from right to left. Going from right to left, first a GaAs buffer layer is grown, then the first set of three QWs and a 100 nm 1% N containing layer. After this, another set of three QWs and on top of this a Si-doped GaAs capping layer. The numbers on the top of the image indicate the different N:GaAs QWs. The N concentrations of QW 1, 2 and 3 are 0.85 %, 0.53 % and 0.35% respectively. The N concentrations of QW 4, 5 and 6 are again 0.85 %, 0.53 % and 0.35% respectively. The numbers in the layers indicate their thickness, while the colors indicate the material. The top half of the structure, from QW 1 to QW 3, is passivated with hydrogen post-growth as indicated by the blue bar at the bottom.

5.2 Hydrogen Passivation Setup and Conditions

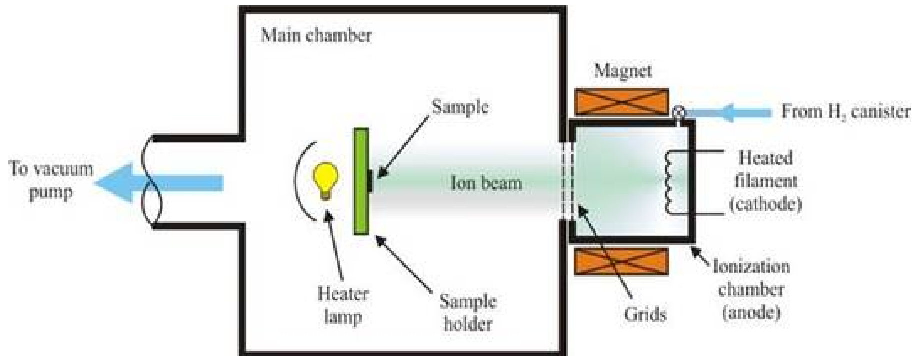

Figure 5.2: Schematic overview of a Kaufman source as used for the hydrogen passivation. Adapted from Ref [65].

Figure 5.2 shows a schematic overview of the Kaufman source used to passivate the samples. Molecular hydrogen is led to the setup, where it is ionized or dissociated into protons. This is achieved by electrons emitted from a hot tungsten filament (cathode) towards the walls of the chamber (anode). The trajectories of these electrons are spiraled by a magnet to enhance the cross-section of the ionization process. The hydrogen ions are then accelerated by a set of high-voltage grids, creating an ion beam with a Gaussian profile (σ ~25 mm) [65]. The ion beam then enters the main chamber and impinges on the sample, which is electrically grounded. A low pressure of $5 \cdot 10^{-7}$ mbar is created in the main chamber by a turbo-molecular pump and during the H-irradiation the pressure is maintained at $3 \cdot 10^{-4}$ mbar. The heater lamp behind the sample provides a way to control the temperature of the sample.

Sample 2131 was fully passivated with an impinging dose of $2.5 \cdot 10^{18}$. The conditions of the passivation should have ensured a mix of N-2H and N-3H complexes. Sample 2233 was partially passivated with a dose of $3 \cdot 10^{17}$ to ensure that QW 1 to 3 are passivated while 4 to 6 are not.

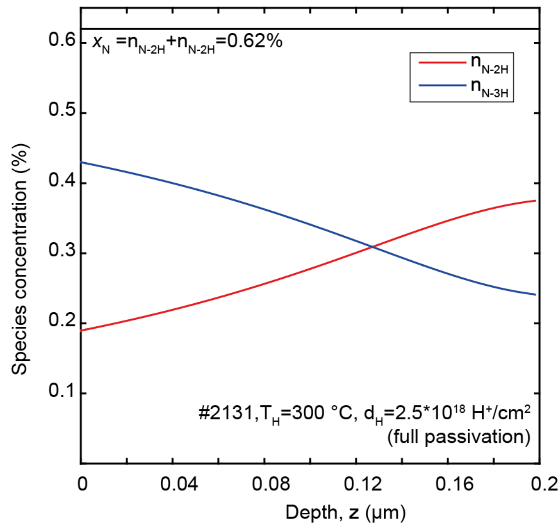

Figure 5.3: Hydrogen passivation simulation of sample 2131, for a sample temperature of 330°C and an impinging hydrogen dose of $2.5 \cdot 10^{18}$. The red and blue line indicate the concentration of N-2H and N-3H complexes respectively.

5.3 Hydrogen Passivation Simulations

To determine the right passivation conditions for the samples, finite element modeling (FEM) simulations of the passivation process have been performed. These simulations are based on the diffusion of hydrogen through the material [40]. Especially for sample 2233 it is important to know the correct parameters for passivation, since the goal is to passivate only half of the structure.

The simulations for sample 2131 indicate that the sample should be fully passivated with a mixture of N-2H and N-3H complexes, as shown in Figure 5.3. The sample temperature of 300°C ensures that a relatively high concentration of N-2H is incorporated in the sample. The blue line indicates the concentration of N-2H complexes as a function of depth, the red line indicates the N-3H concentration. The total concentration adds up to the N concentration in the sample, indicating the full passivation. Starting from zero depth the N-3H complex is the main species present. The concentration of N-3H slowly decreases going deeper into the sample and around z = 130 nm, N-2H becomes the main species.

For sample 2233 QW 1 to 3 should be fully passivated as illustrated in Figure 5.4 by the fact that the hydrogen species concentration is equal to the N concentration of the QWs. The main species present in QW 1 to 3 is N-3H. This is ensured by the sample temperature of 250°C. The passivation is terminated in the 1% N layer in the middle of the sample, which is accompanied by a small distribution of N-2H around the front. QW 4, 5 and 6 should contain no NH-complexes at all.

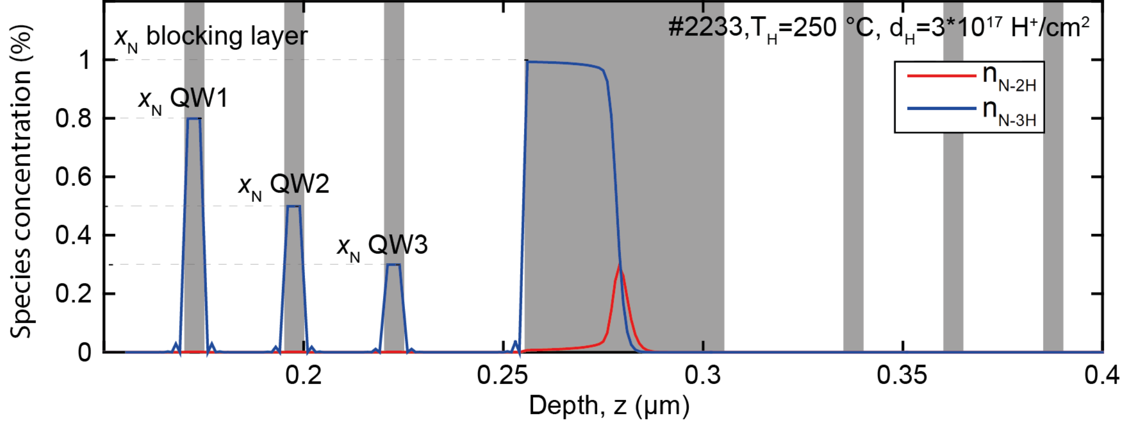

Figure 5.4: Hydrogen passivation simulation of sample 2233, for a sample temperature of 250°C and an impinging hydrogen dose of $3 \cdot 10^{17}$. The red and blue line indicate the concentration of N-2H and N-3H complexes respectively.

5.4 Photoluminescence

PL is used as a relatively easy method to check if the hydrogen passivation is successful. Room temperature PL spectra of the samples are measured before and after the passivation to compare them.

5.4.1 Sample 2131

For sample 2131 no reference spectrum was recorded. Instead, a reference spectrum was made of sample 2233. The structure of this sample is the same as 2131, but the N concentration is 0.39 % instead of 0.62 %. The spectrum of 2132, as displayed in Figure 5.5(a), shows a two-peak structure, with one peak at 870 nm and the other at 930 nm. The peak at 870 nm is attributed to emission from GaAs, since the bandgap of GaAs at room temperature is 1.42 eV (872 nm). The other peak originates from the N:GaAs layer.

The sample was passivated with an impinging hydrogen dose of $2.5 \cdot 10^{18}$, with conditions that should have ensured a mix of N-2H and N-3H complexes. After the passivation the N:GaAs peak has disappeared, indicating a full passivation of the N:GaAs layer. The GaAs peak is still visible at the same wavelength as before the passivation.

5.4.2 Sample 2233

Both the reference spectrum and the spectrum after passivation of sample 2233 are displayed in Figure 5.5(b). The sample shows a N:GaAs related peak around 920 nm and the GaAs peak at 865 nm. Since the QWs of this sample have different concentrations of N, they should emit at different energies. Unfortunately this could not be observed in the PL spectrum, only a broad N:GaAs related peak is observed.

After an impinging hydrogen dose of $3 \cdot 10^{17}$ the N:GaAs peak has completely disappeared and the GaAs peak has shifted to 870 nm. This hydrogen dose should have ensured the full passivation of QW 1 to 3, while QW 4 to 6 remain non-passivated. Since the emission from the different QWs cannot be distinguished, it not possible to determine which of the QWs have been passivated.

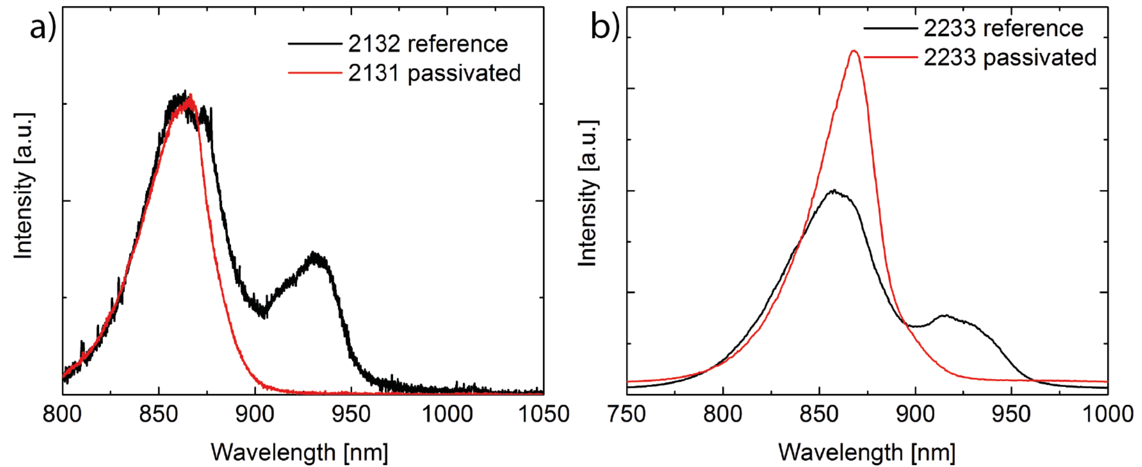

Figure 5.5: Room temperature PL spectra obtained of sample 2131/2132 (a) and 2233 (b), before and after passivation. There is no reference spectrum of 2131, instead the PL spectrum of a similar sample (2132) is shown. This sample has the same structure are 2131, but a 0.39 % N concentration in the N:GaAs layer. The spectra in (a) are peak-normalized, while the spectra in (b) are normalized with a reference sample.

5.5 Conclusion

PL measurements of both N:GaAs samples prepared for XSTM measurements indicated hydrogen passivation. For sample 2131 the passivation conditions should have ensure a mixture of N-2H and N-3H complexes. The PL spectrum of this sample after passivation showed no PL peak at all from the N:GaAs layer, indicating a full passivation. Sample 2233 was passivated under conditions that should have ensured full passivation of QW 1 to 3 without passivating QW 4 to 6. The passivation of the sample was confirmed by PL measurements, but since emission from the separate QWs could not be distinguished it is not possible to say if QW 1, 2 and 3 are all passivated. Simulations of this passivation indicate that QW 1 should contain a high concentration of N-3H complexes, while QW 2 and 3 should contain primarily N-2H.

Chapter 6

Hydrogen passivation tests at TU/e

Our collaboration with the group of Marco Felici has been very successful, and they have extensive knowledge of the hydrogen passivation process of N:GaAs. But there is always an added convenience with collaboration within our own university. Especially with the available expertise of hydrogen plasmas of the Plasma and Materials Processing (PMP) group. While they do not have the same hydrogen source available, it is interesting to see if the passivation process can also be performed with other sources.

This chapter will focus on the hydrogen passivation tests performed at the TU/e. These tests were performed on an N:GaAs and an Sb:GaAs sample simultaneously and the effects of the passivation were studied using PL and XRD. Since the PL and XRD signatures of passivated and non-passivated N:GaAs are well documented in literature it provides a way to confirm whether the passivation was successful or not. The effects of hydrogen passivation on Sb:GaAs have, to our knowledge, not yet been studied.

6.1 Sample Information

Samples were grown with molecular beam epitaxy (MBE) by Alicia Gonzalo in the group of Jose María Ulloa at the Institute for Optoelectronic Systems and Microtechnology of the Universidad Politécnica Madrid. The N:GaAs sample has a Si-doped GaAs substrate, followed by a 250 nm GaAs buffer layer, a 200 nm 0.85% N layer and a 100 nm GaAs capping layer. The Sb:GaAs sample has an n-doped GaAs substrate, a 250 nm GaAs buffer layer and a 200 nm Sb:GaAs layer with 7.1% Sb.

6.2 Hydrogen Plasma Source and Conditions

Hydrogen passivation was performed by Karsten Arts in the PMP group of professor Erwin Kessels at the TU/e. The machine used for the hydrogen passivation is a FlexAl2 with substrate biasing, made by Oxford Instruments Plasma Technology.

The samples were exposed to a hydrogen plasma two times, under conditions as listed in Table 6.1. PL and XRD-RC measurements were performed on the as-grown samples and after each exposure. A part of each sample was kept separate and never exposed to the hydrogen, to act as a reference sample.

	Exposure 1	Exposure 2
Sample temperature	300°C	300°C
Pressure	30 mTorr	9 mTorr
ICP power	300 W	600 W
RF bias power	6 W	6 W
Ion energy range	60 - 105 eV	65 - 115 eV
Ion flux	$4 \cdot 10^{14}$ cm^{-2}s^{-1}	$10 \cdot 10^{14}$ cm^{-2}s^{-1}
Ion current density	64 μA/cm^2	64 μA/cm^2
Exposure time	1 h	4 h
H+ dose	$1.4 \cdot 10^{18}$	$1.4 \cdot 10^{19}$

Table 6.1: Hydrogen passivation conditions

6.3 Hydrogen Plasma Exposures

6.3.1 PL

PL is obtained by exciting the samples with a 635 nm laser and analyzing the emitted light using a spectrometer. All PL measurements are performed at 10 K, have a background spectrum subtracted and the spectra are normalized using the peak intensity of the reference sample, allowing us to compare absolute intensities. The excitation powers were determined by measuring the incident power just before the beam enters the cryostat.

Figure 6.1(a) displays the PL spectra of the N:GaAs sample before and after each exposure to the hydrogen plasma at an excitation power of 7.1 μW. The as-grown sample exhibits two peaks, one around 830 nm and one around 970 nm. The 830 nm (1.51 eV) peak arises from the band to band recombination of GaAs at 10 K, while the peak at 970 nm is attributed to the N:GaAs layer. In the GaAs peak a dip can be observed at 819 nm, this is an absorption line caused by the electron-hole plasma created at high excitation powers [66].

After the first exposure the overall intensity of the PL decreases, but the two-peak structure of the spectrum remains. The ratio between the N:GaAs and GaAs peak has decreased about 4 times and for excitation powers below 1 μW the GaAs peak is now larger than the N:GaAs peak, as can be seen in Figure 6.2. This change in peak ratio in favor of the GaAs peak could be a first indication of passivation of the N:GaAs layer. Since the N:GaAs peak is still visible it can be assumed that the layer is not fully passivated. After the second exposure the shape of the PL spectrum shows a major change, with the GaAs and N:GaAs disappearing and a new peak appearing around 875 nm. The new peak has a long tail to longer wavelengths and the intensity of this peak is more than an order of magnitude higher than the previous spectra.

Figure 6.1(b) displays the PL spectra of the Sb:GaAs obtained at an excitation power 7.1 μW. The as-grown spectrum shows two peaks, around 838 nm and 923 nm. The peak around 838 can be attributed to the band to band recombination of GaAs and the 923 nm peak to the Sb:GaAs layer. The Sb:GaAs peak shows a high shoulder at the short wavelength side and a low, broad shoulder at the long wavelength side.

After the first exposure to the hydrogen plasma both peaks are still visible with decreased intensity, but the GaAs peak has redshifted to 845 nm while the Sb:GaAs peak has blueshifted to 909 nm. The ratio between the peaks for different excitation powers showed no clear trend. The decreasing distance between the GaAs and Sb:GaAs peak might be an effect caused by hydrogen passivation of the sample. The second exposure completely changes the spectrum, the GaAs and Sb:GaAs disappear and a single peak shows around 860 nm. The intensity of this new peak is close to an order of magnitude more intense than the previous spectra and it shows a long tail towards longer wavelengths.

The complete disappearance of the N and Sb peaks after the second exposure could indicate that the both samples are fully passivated. But the spectra obtained after the second exposure do

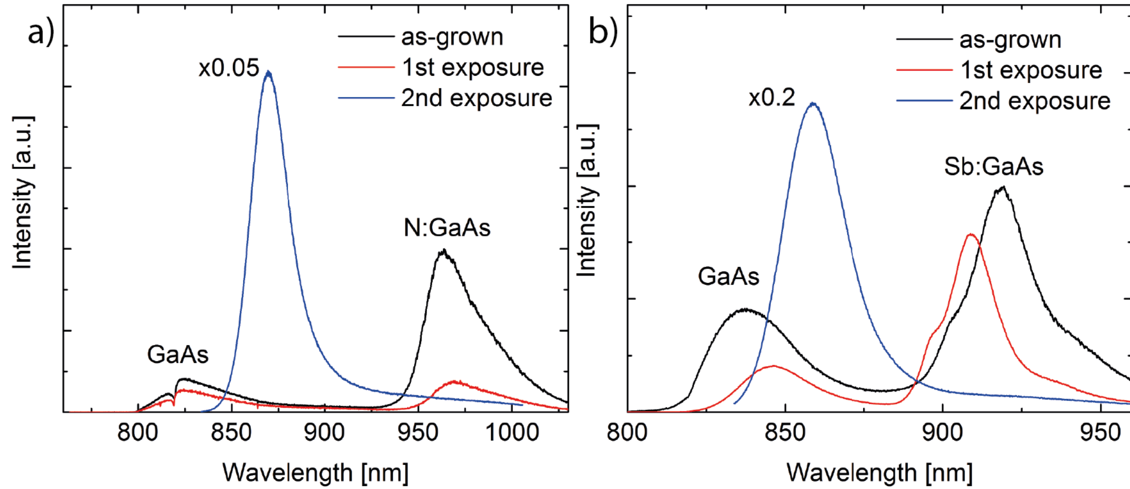

Figure 6.1: PL of the N:GaAs (a) and SbGaAs (b) sample, as-grown and after each exposure, obtained with a incident power of 7.1 μW. Spectra are normalized with a reference sample. The spectra after the second exposure are scaled down to increase the readability of the graph.

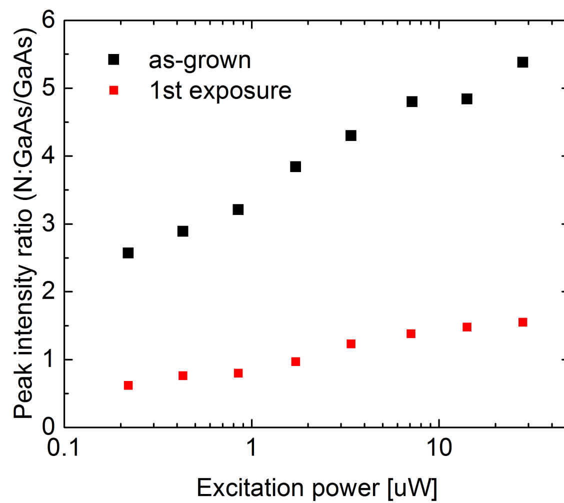

Figure 6.2: Ratio between the intensity of the N:GaAs and GaAs peak before and the first exposure

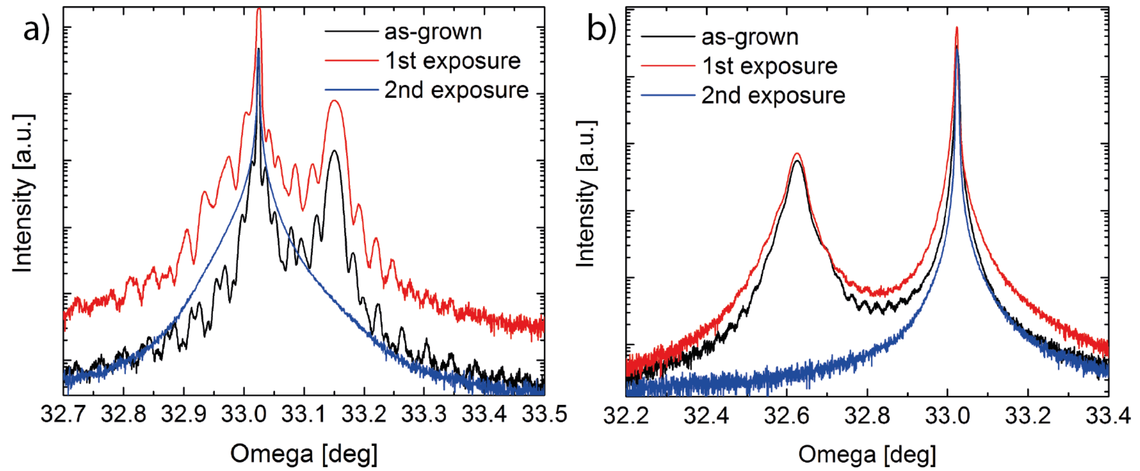

Figure 6.3: XRD-RCs of the N:GaAs (a) and Sb:GaAs (b) sample before exposure to the hydrogen plasma (black), after the first exposure (red) and after the second exposure (blue)

not match with literature [48]. The similarities between the spectra of N:GaAs and Sb:GaAs after the second exposure might indicate that the grown layers of the samples have been etched away by the hydrogen plasma, leaving only a hydrogen influenced GaAs sample. The large increase in PL intensity could in this case be explained by the hydrogen passivation of defects in GaAs [29].

6.3.2 XRD rocking curves

XRD rocking curves (XRD-RCs) were obtained on the as-grown samples and after each hydrogen exposure. The results for the as-grown N:GaAs sample are displayed in Figure 6.3(a), here the main GaAs peak can be seen at 33.05 deg and the N peak is visible around 33.15 deg, which is good agreement with the results obtained in Ref [50]. The presence of the epilayer structure can be observed by oscillations (fringes) of the signal, caused by the interference of the x-rays in the grown layers. After the first exposure the N peak is unaffected and a vague shoulder appeared on the left side of the GaAs peak around 32.95 deg. After the second exposure the N peak has completely disappeared and with it the oscillations in the signal.

The XRD results of the Sb:GaAs are displayed Figure 6.3. The as-grown sample shows a peak around 33.05 deg attributed to the GaAs, and a peak around 32.65 deg attributed to the Sb:GaAs. The fringes caused by the epilayers can also be observed. After the first exposure no significant change is observed in both peaks, but the intensity of the fringes has decreased. The second exposure caused the Sb:GaAs peak to completely disappear, leaving only the GaAs peak at 33.05 deg. The fringes have also completely disappeared.

The vague shoulder at 32.95 deg appearing for the N:GaAs sample after the first exposure is an effect also observed in Ref [50], although there it is much more pronounced. This could mean that the first exposure has only partially passivated the sample. The complete disappearance of the N and Sb peaks, and also the fringes, after the second exposure support the possibility that the epilayers have been etched away and only hydrogen-influenced GaAs remains.

6.4 Annealing

To check if the major effects observed in PL and XRD after the second exposure to the plasma can be reversed, the samples are annealed. The exposed samples are split and one part is annealed at 250°C for 6 hours and 30 minutes and the other part at 330°C for 3 hours and 15 minutes. These temperatures were chosen because they are reported to be the temperatures where the N-2H (330°C) or N-3H (250°C) complexes in passivated N:GaAs disassociate [50].

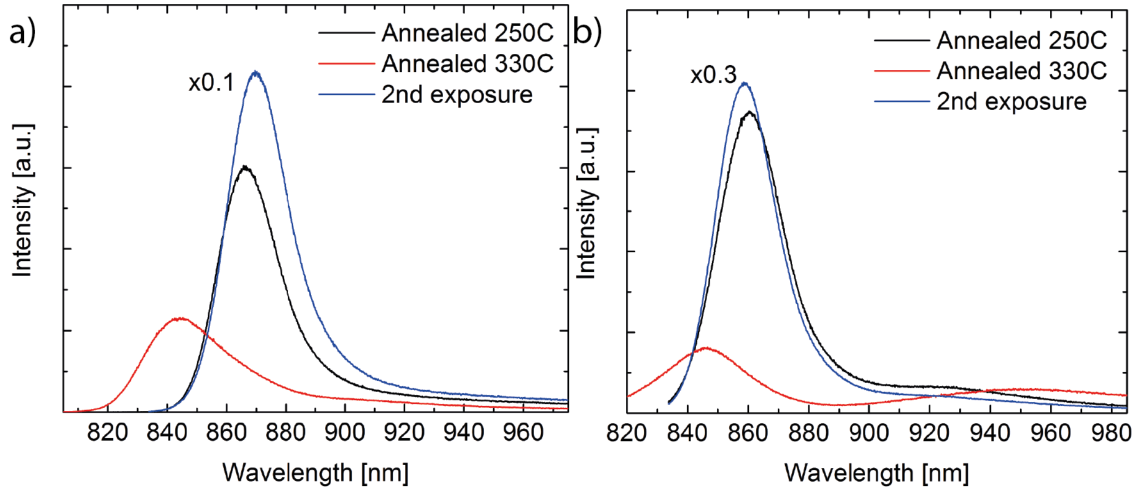

Figure 6.4: PL of N (a) and Sb (b) after the second exposure to the hydrogen plasma (blue) and after annealing at either 250°C (black) or 330°C (red) obtained with an excitation power of 7.1μW. The spectra after the second exposure are scaled down to improve the readability of the figure graph.

The results for the N:GaAs sample are displayed in Figure 6.4(a). After the 250°C annealing the intensity of the PL has decreased by more than an order of magnitude, the peak shows a blueshift to 865 nm and the tail at longer wavelengths remains. The annealing at 330°C also strongly decreases the PL intensity and the peak is blueshifted to 845 nm.

The PL spectra of the Sb:GaAs sample are displayed in Figure 6.4(b). After annealing the sample at 250°C the intensity decreases strongly and the long wavelength shoulder gets more pronounced. The peak energy shows a small redshift. The 330°C annealing causes a blueshift of the peak to 847 nm and the appearance of a broad peak around 950 nm.

For both samples their previous PL properties do not get restored after annealing, further supporting the theory that the samples have been etched by the second exposure. The same goes for the fact that the spectra for the different show a similar behavior with the annealing. The broad peak appearing in the Sb:GaAs sample around 950 nm might be a signature of some remaining Sb, but this is very much a speculation. In general the 330°C annealing has a larger effect on the samples, even though the annealing time was only half as long.

The strong decrease of the PL intensity for both annealings can be linked to the passivation of defects in GaAs [29]. As a result of the annealing the passivation could be removed, reactivating the defects. They can now act as traps for carriers, decreasing the PL efficiency.

6.5 Conclusion

We exposed a N:GaAs and a Sb:GaAs sample to a hydrogen plasma to try and passivate them. After the first exposure weak indications of passivation are observed in both samples by PL and XRD-RC measurements. For the N:GaAs sample the indications for passivation are a 4 times decrease in the ratio between the GaAs and N:GaAs PL peak, and a vague shoulder appearing in the XRD-RC measurement. For the Sb:GaAs sample the indication for passivation is a decrease in the distance between the GaAs and Sb:GaAs peak. A second exposure, with a higher hydrogen dose, has likely damaged the samples, causing a complete disappearance of the N and Sb peaks in XRD-RC measurements. In PL this is visible in both samples by the disappearance of the GaAs and N/Sb:GaAs peaks and the appearance of a single peak around 860 nm. Thermal annealing was performed on the samples after the second hydrogen exposure. Annealing at 250°C showed a decrease in PL intensity of an order of magnitude, but has little effect on the peak position. The

330°C annealing caused a blueshift of the PL peak to around 845 nm in both samples. In the Sb:GaAs a broad peak appeared around 950 nm, which might originate from remaining Sb, but further research needs to be done to gain a better insight in this.

6.6 Outlook

To check whether the samples have been damaged by the second hydrogen exposure, we can compare the surface of these samples with the reference samples. This could easily be done with an optical microscopy, but for a more detailed view scanning electron microscopy would be good option. For a new hydrogen passivation run it is interesting to repeat the conditions of the first exposure, but extend the time by a few hours. Because we observed indications of partial passivation with a 1 hour exposure, longer exposures might make these indications more significant. Since the annealing at 330°C had a larger effect, it would be interesting to perform this annealing for a longer time and see what the effects are. By doing this on the same samples we can try to obtain a general trend in the changes in the spectra during the annealing. With this we could also check if the broad PL peak around 950 nm in the Sb:GaAs samples gets more pronounced.

Chapter 7

XSTM study of hydrogen passivated N:GaAs

The goal of this research is to directly study NH-complexes formed in hydrogen passivated N:GaAs at the atomic level. This chapter will present the results obtained from XSTM measurements with atomic resolution on hydrogen passivated N:GaAs. First the features observed in the passivated layers are described in detail. Then it is discussed if, and how, hydrogen passivation affects the contrast of N atoms in XSTM measurements. Afterwards some general observations made when measuring on passivated N:GaAs are discussed. And lastly we speculate what the exact configurations of the NH-complexes could cause the observed features.

7.1 Observed Features

To get an indication of the changes that hydrogen passivation introduces in N:GaAs, some large overview images were made. Figure 7.1 displays such an overview the thick bulk-like N:GaAs layer of sample 2131. The STM image displayed there measures 80 by 80 nm. On the right side of the image the end of the GaAs buffer layer is visible, the rest of the image contains the hydrogen passivated 0.62% N layer. Crystal directions were determined by the growth direction of the sample and comparison with known N features from Refs [17] [61]. Large extended dark and bright features in the $[1\bar{1}0]$ direction are ripped out rows of atoms (dark) and rows of atoms left behind (bright) induced by the imperfect cleaving of the sample. N atoms in the first (surface) and third layer are visible as dark features with the size of one anion unit cell. Additionally, the image contains a wide variety of features not observed in non-passivated N:GaAs samples, of which three main types will be discussed in the following section. Although there are more types present in the hydrogen passivated layer, their rate of appearance is much lower than those three.

The discussion of the three features will be done by zooming in on an area of Figure 7.1 marked by the white rectangle and displayed in Figure 7.2. In Figure 7.2 the numbers 1 and 3 mark substitutional N atoms in the first and third plane as identified by the characteristics mentioned in [16] [59] [60]. The three main features are marked with A, B(1/2) and C(1/2).

A voltage series in the range between -3.2 and -2.2V showed no change in the contrast of feature A, B and C, indicating that they originate from structural effects and not from electronic effects, which typically occur at specific voltages. These three features are also observed in sample 2233, but they are flipped 180 degrees with respect to the growth direction. This is due to the fact that cleaving the sample either reveals the (110) or the $(1\bar{1}0)$ plane, depending on the orientation. The difference between these two planes lies in the orientation of the Ga and As rows, as explained in Section 3.5. For one plane the closest Ga row is located on the [001] side of the As row, while for the other the closest Ga row is on the $[00\bar{1}]$ side. The crystal orientation was unknown when preparing the samples, resulting in a 50 % chance of cleaving either surface.

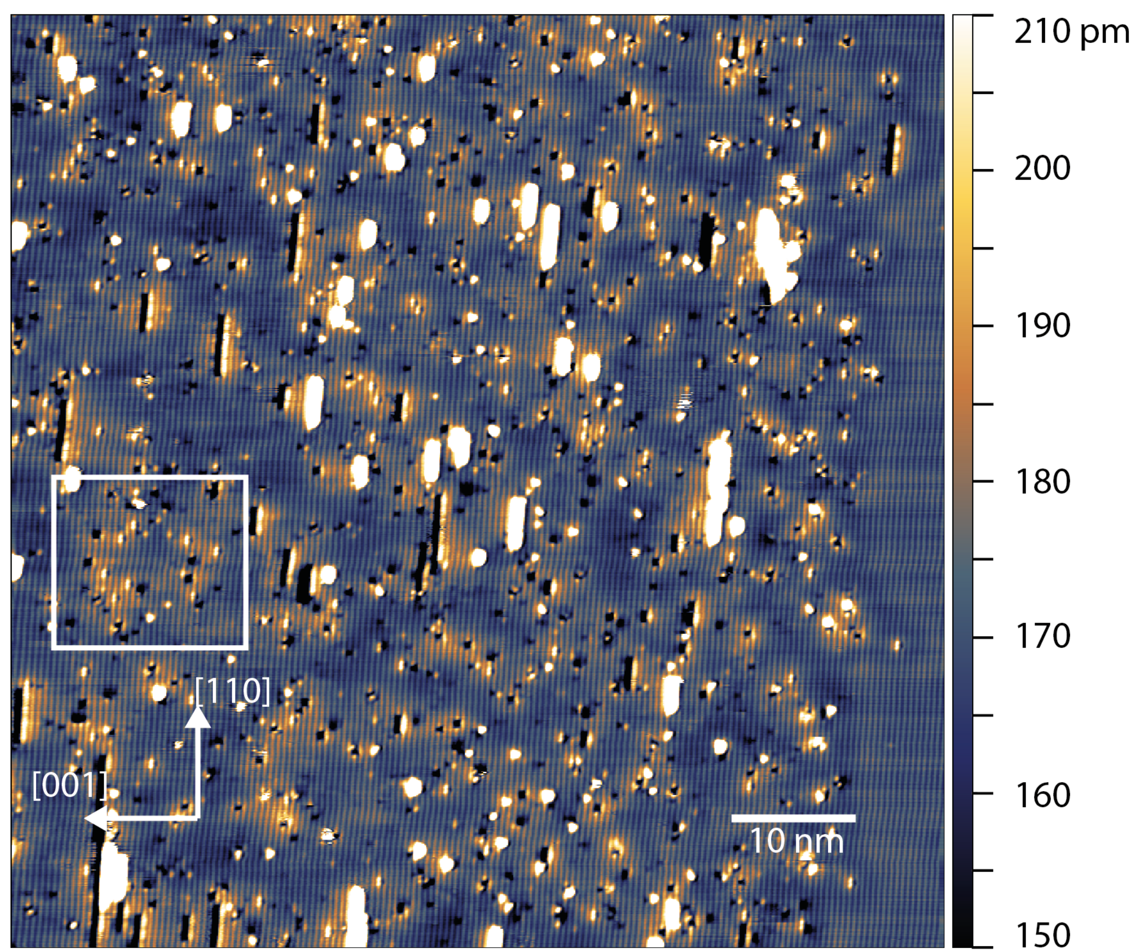

Figure 7.1: Filled state STM image of a 80x80 nm area of sample 2131. Large extended bright and dark features in the [110] direction are ripped out rows of atoms (dark) and rows of atoms left behind (bright) induced by cleaving the sample. The white rectangle marks the area displayed in Figure 7.2. (-3.35V, 30pA, 77K)

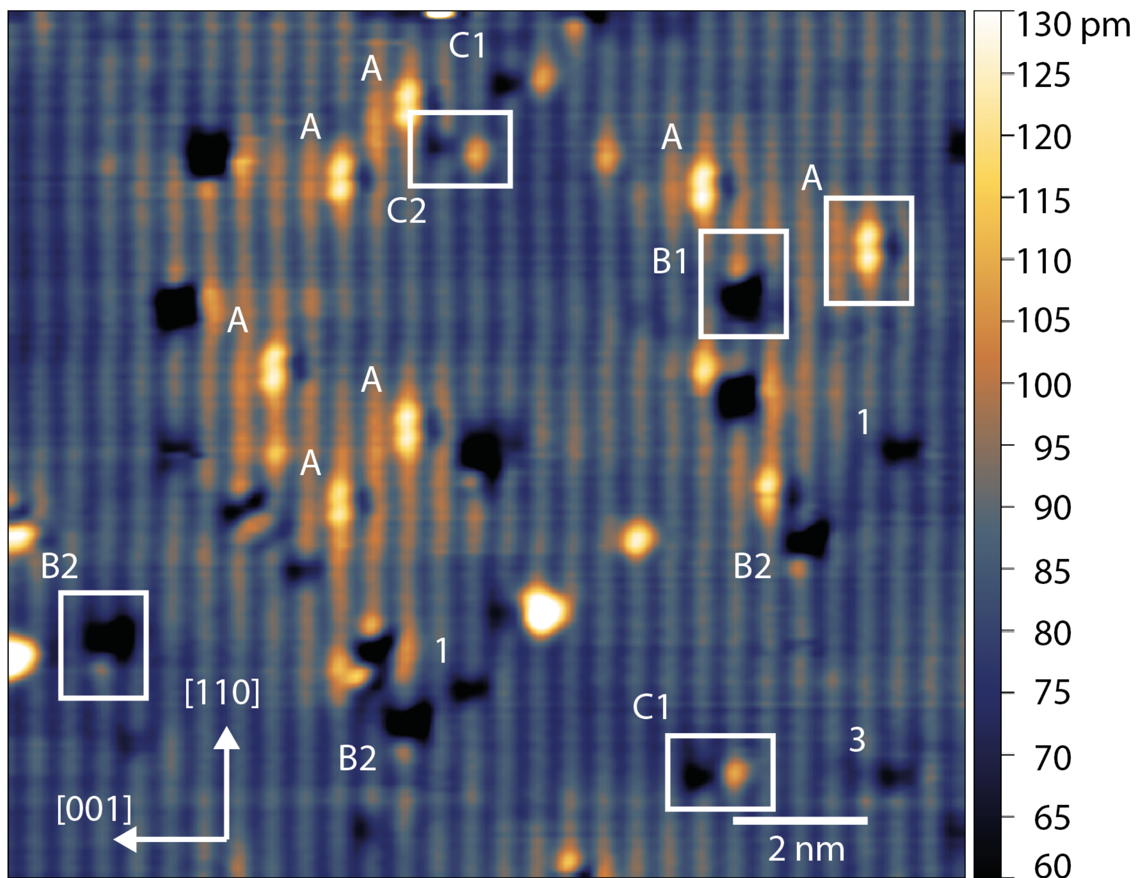

Figure 7.2: Filled state STM image of hydrogen passivated N layer. 1 and 3 mark substitutonal N atoms in the first (surface) and third plane. Main observed features are marked with A, B(1/2) and C(1/2) and one of each of the features is marked with a white rectangle. (-3.35V, 30pA, 77K) (29-03-2018)

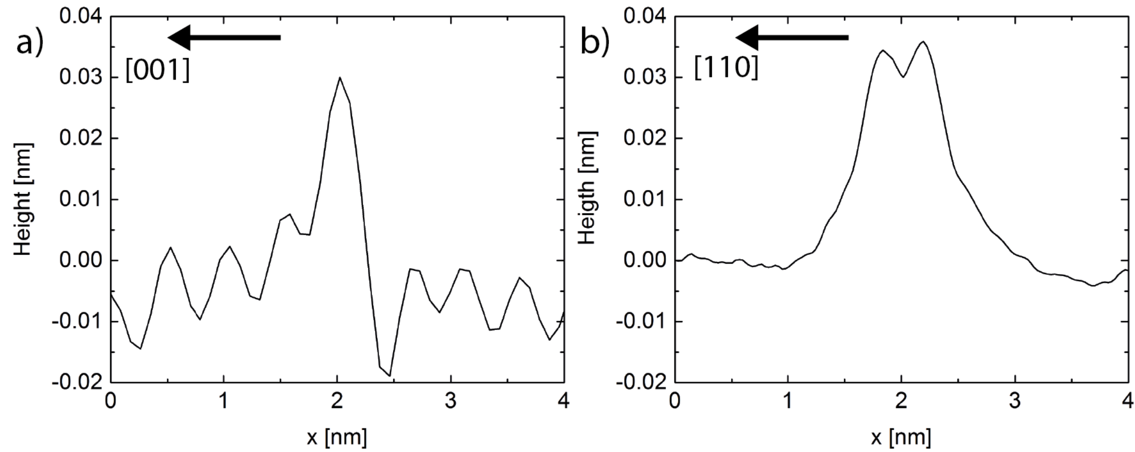

Figure 7.3: Height profile of feature A in [001] (a) and [110] (b) direction, arrows in the graph indicate the crystal directions. Profiles are obtained by taking the average over three features.

The three main features will be described below, with regards to their shape and other properties.

7.1.1 Feature A

Feature A has a bright dumbbell-like shape with its long axis along the [110] direction and is located on a corrugation line. Height profiles of this feature are displayed in Figure 7.3, with (a) taken along the [001] direction and (b) along the [110] direction. In the $[00\bar{1}]$ direction, next to the middle of the long axis, a small depression of the surface appears. This depression is located between the corrugation lines and is about 0.01 nm deeper than the normal depth of the area between the corrugation lines. The long axis of the feature, along the [110] direction, spans around 1 nm, corresponding to twice the lattice constant of GaAs. The feature is at its maximum, 0.035 nm higher than the (110) plane and has a small dip of about 0.005 nm in the middle of its long axis. Under normal scanning conditions (-3V, 30pA) the feature can move over the GaAs(100) surface in both the [001] and [110] directions. During movement it always keeps its long axis in the [110] direction and its main contrast remains on the corrugation lines, as is illustrated in Figure 7.4.

The same feature has been observed in the supplementary information of Ref [61], where it is classified as a surface adsorbate. Since the samples in Ref [61] were not passivated with hydrogen, it is likely that feature A is indeed purely N related. The occurrence of this feature is much higher on passivated N:GaAs samples (192 observed in 135x50 nm), indicating that the passivation influences the occurrence. Since the passivation breaks two N-Ga bonds, it is possible for N atoms in the first layer of the cleaved surface to have only one N-Ga bond remaining. One could imagine that this raises the probability that N atoms leave their "embedded" position in the lattice and become an adsorbed atom residing on top of the cleaved surface.

7.1.2 Feature B

Feature B is a depression of the surface on a corrugation line with a neighboring bright dot in the same corrugation line. This bright dot can be in the [110] (B1) or $[\bar{1}\bar{1}0]$ (B2) direction. In an 135x50 area of the sample 40 occurrences of B1 were observed and 41 of B2. Figure 7.5(a) displays the height profile of a first layer N atom (black), feature B (red) and a ripped out row of atoms (blue) along the [001] direction. On the left side the figure oscillations are visible as a result of the corrugation lines. The profiles for the different features are aligned and set to zero based on the last corrugation line before the features. The first layer N atom shows a depression

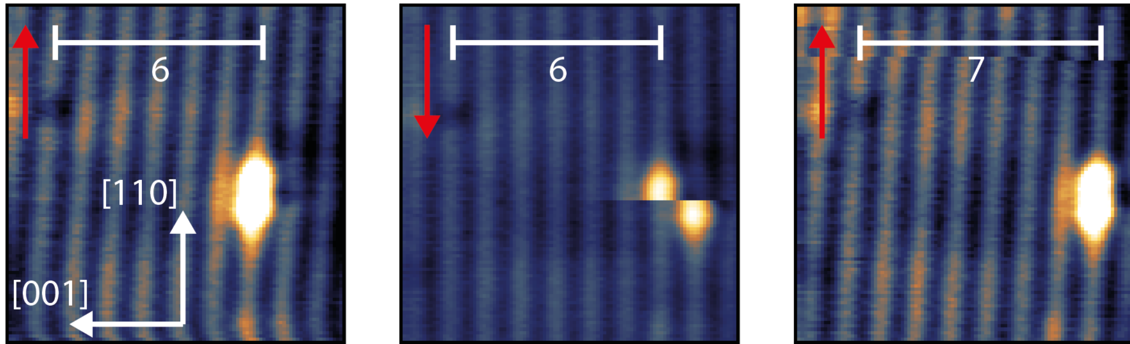

Figure 7.4: Dragging of feature A as captured in three consecutive images, red arrows indicate the slow scanning direction. The number under the distance bar indicates the number of corrugation rows the dumbbell is removed from the N feature in the top left of the image. In the middle image the feature suddenly moves to the neighboring corrugation line in the $[00\bar{1}]$ direction. (-3V 30pA 77K)

of about 0.03 nm compared to the top of the corrugation line, with a small bump in the middle of the depression. Feature B has a depth of about 0.07 nm and no bump in the middle. Compared to a non-passivated 1st layer N atom, feature B is more than twice as deep, but it is not as deep as a ripped out row of atoms, which is 0.09 nm deep.

Taking spectroscopy on feature B often has no effect, the contrast profile remains at the same position in the lattice and retains its shape. In one case we observed that feature B could be made to switch back and forth between B1 and B2 during spectroscopy measurements as illustrated in Figure 7.6. Between each image a spectroscopy curve was taken on the feature causing it to change from B1 to B2 and vice versa.

The height profiles of feature B1 and B2 taken from sample 2233 are displayed in Figure 7.5(b). The profiles are the result of averaging the height profile of three features for each line and zero height is defined by the last corrugation line before the depression. In the figure it can be observed that feature B2 is slightly deeper than B1. The absolute difference in depth is 0.0023 nm, with B2 being 7.9% deeper than B1. The depth difference is also observed in sample 2131, but both features are deeper and as a result the absolute difference is 0.0106 nm and the relative difference 17.4 %. Since measurements were performed with different tips and the features are flipped 180 degrees, the probability that the depth difference between the features is only caused by the tip shape or scanning direction is unlikely.

7.1.3 Feature C

Feature C shows as a depression of the surface within a corrugation line with a bright dot in the neighboring corrugation line in the $[00\bar{1}]$ direction. This bright dot has a slight displacement in the [110] (C1) or $[\bar{1}\bar{1}0]$ (C2) direction relative to the depression of the surface, with 48 times C1 and 54 times C2 appearing in a 135x50 nm area of the sample. The depression has the same characteristic depth as an N atom in the first layer of the surface.

By taking spectroscopy curves on the feature, the bright dot can be removed, leaving behind a feature looking like a normal 1st layer N as illustrated in Figure 7.7. The voltage range for these spectroscopy measurements usually ran from -3 V to +2.5 V. The depression of the surface caused by the N atom is on average 0.05A deeper after removal of the bright dot, which could either be a physical change in the depth of the surface or be caused by the feature getting wider in the [001] direction and as a result allowing the tip to follow the depression better.

Feature B could be switched during spectroscopy measurements, while C can be removed. This is an indication of a difference in bond strength of the atoms involved in feature B and C. Feature C seems to have a lower bond strength, as the feature can be removed.

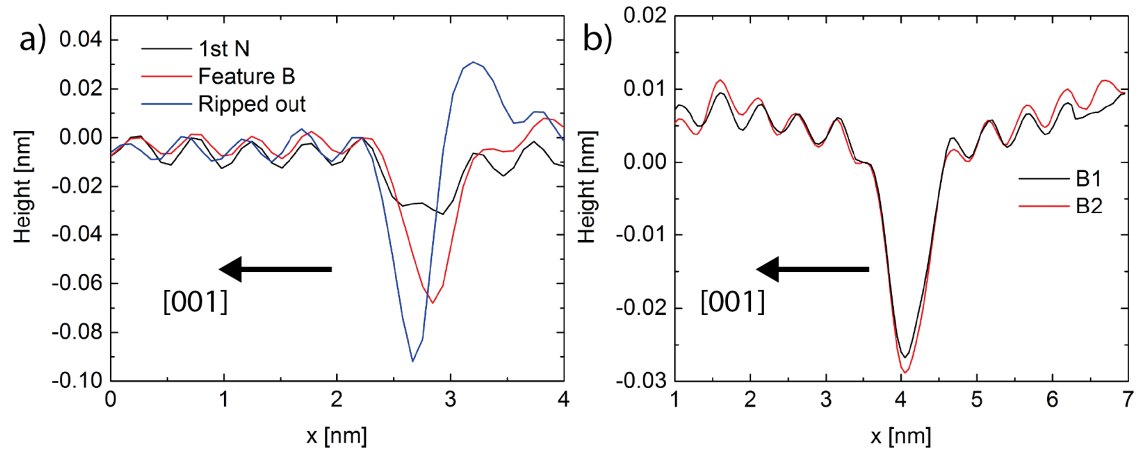

Figure 7.5: (a) Height profiles of a 1st layer N, feature B and a ripped out row of atoms. All profiles were obtained from sample 2131 by taking the average profile of three features. Zero height is set at the top of the last corrugation line before the features. (b) Height profiles of feature B1 and B2 obtained by averaging over three features for each line, taken from sample 2233.

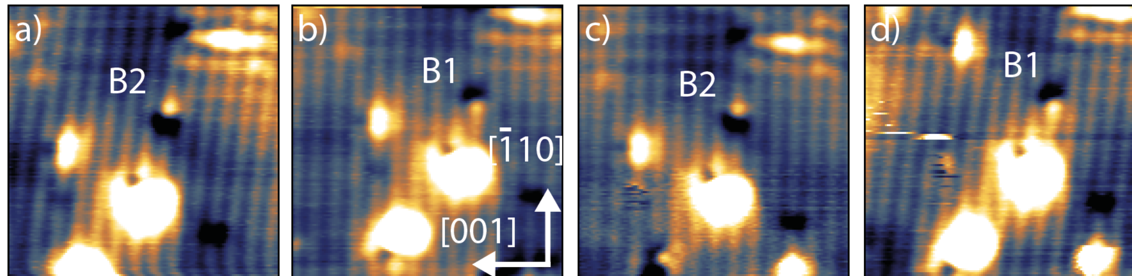

Figure 7.6: Switching of feature B from B2 to B1 and back by taking spectroscopy curves on the feature. Between each image a spectroscopy curve was performed from -3V to +2.5V. (-3V, 30pA, 77K)

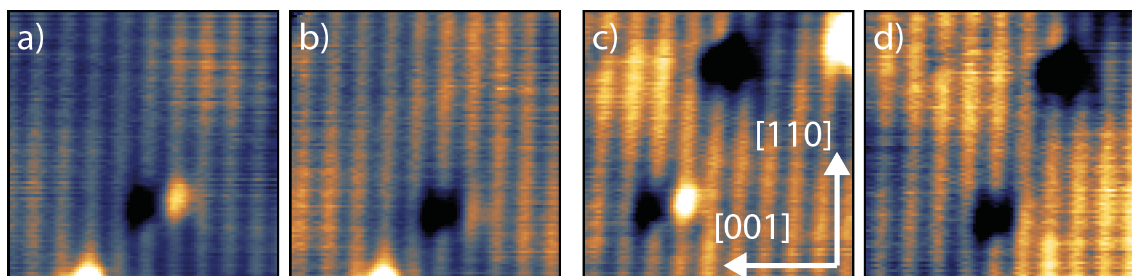

Figure 7.7: Removal of the bright dot from feature C1 by taking spectroscopy curves. The process is shows for two separate features, with (a) and (b) showing one feature before and after removal and (c) and (d) showing another feature before and after removal.

7.2 Feature Related Observations

The previous section gave a description of the features observed in passivated N:GaAs layers. In this section we will discuss observations directly linked to these features and try to match them to specific NH-complexes.

7.2.1 Filled State Imaging

For this discussion it important to know where feature A, B and C were observed in sample 2233. For this purpose a filled state image of QW 1 and 2 of sample 2233 is displayed in Figure 7.8. In QW 1 a B1 and C1 feature are marked with a white rectangle. In this specific image and in an area stretching 500 nm along the QWs, none of the passivation related features (A, B and C) were observed in QW 2 and 3. In this same area, multiple of these features were observed in QW 1. Additionally, when comparing QW 2 and 3 to the non-passivated QWs 4 to 6, no difference is observed and all N related features look the same as non-passivated N atoms.

The simulations of the passivation indicated that QW 1, 2 and 3 are all fully passivated with N-3H complexes, as explained in Section 5.3. According to the simulations the N-3H front ends in the middle of the thick 1% N layer, with a distribution of N-2H being present at this front. PL measurements on sample 2233 show full disappearance of the N:GaAs peak, but since luminescence from the separate QWs could not be distinguished it could not be determined which specific QWs were passivated.

Somehow there is a discrepancy between the STM measurement (where feature B and C are only observed in QW 1 and not in 2 and 3) and the simulations (which suggest that QW 1, 2 and 3 are all fully passivated with N-3H). Three scenarios can be envisioned for this. Either the hydrogen front did not progress far enough into the sample and QW 2 and 3 are not passivated (scenario 1). Or QW 1,2 and 3 are fully passivated, but QW 1 is passivated with primarily N-3H while QW 2 and 3 are passivated with N-2H. If feature B and C are related to N-3H complexes this would explain why they are not observed in QW 2 and 3. This theory still leaves two scenarios open for the XSTM contrast of N-2H. Either N atoms passivated with N-2H show no contrast at all, and the surface at the location of this feature would look like undisturbed GaAs (scenario 2), or a passivated N atom in a certain layer looks the same as its non-passivated counterpart (scenario 3). We will now discuss the likelihood of each of these scenarios.

Scenario 1) The PL peaks of the separate QWs could not be observed, only a single N related peak showed up in the PL spectrum as shown in Figure 5.5. This peak did disappear after the passivation, indicating that some part of the sample is passivated, but there is no direct evidence that QW 2 and 3 are both passivated. Since QW 4, 5 and 6 should not be passivated, they should still emit at the N:GaAs wavelength. Because this does not show in the PL measurements after passivation, we can assume that the penetration depth of the laser is not large enough to probe these deeper QWs. This could also mean that the laser was only able to probe QW 1 and as a result the full disappearance of the N:GaAs PL peak would only be an indication of full passivated of QW 1. If the passivation front did indeed not progress beyond QW 1, it could be that QW

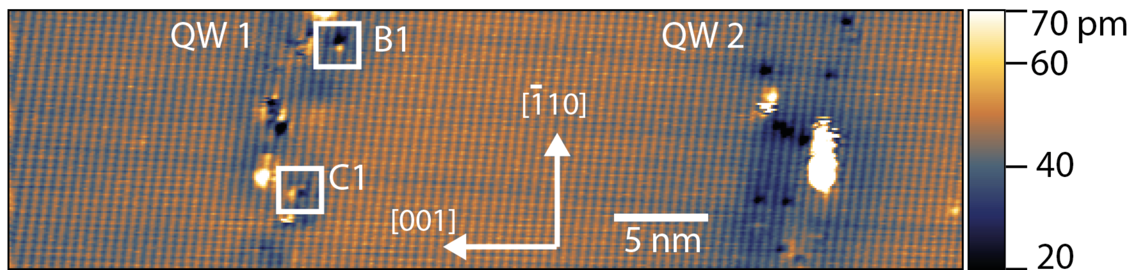

Figure 7.8: Filled state image of QW 1 and 2 of sample 2233. In QW1 a B1 and C1 feature are marked with a white rectangle.

1 is passivated with a mixture of N-2H and N-3H, as the front in Figure 5.4 also shows such a distribution.

Scenario 2) To check whether the contrast of N atoms at filled state imaging completely disappears with passivation, the concentration of N in QW 2 is calculated. By comparing this concentration with the one the growers have determined, we can determine if there are much less N atoms observed in the QW than expected. According to the growers the N concentration in QW 2 is 0.53±0.05 %, as estimated by XRD. By counting the observed 1st and 3rd layer N atoms in STM images of QW 2, the concentration of N atoms was determined to be 0.68%. Since the observed concentration of N atoms in QW 2 is close to the XRD estimated value, it is very unlikely that passivation causes the N atoms to show no contrast at all in filled state images.

Scenario 3) Hydrogen passivation breaks two N-Ga bonds, allowing the N atom to relax in the lattice. This relaxation of the lattice most likely has an effect on how the N atom is observed at the surface. But DFT or tight-binding calculations, which can estimate the effect of this relaxation on the (110) surface, have not been performed.

To summarize: we cannot say with certainty that QW 2 and 3 are passivated, it is very unlikely that passivated N atoms show no contrast in filled state imaging and the theory that hydrogen passivation has no influence at all on contrast of the N atoms is unconfirmed but unlikely. The most likely cause for the discrepancy between the XSTM measurements and the passivation simulations seems to be that QW 2 and 3 are not passivated.

The other question to consider is whether feature B and C are the effect of N-2H or N-3H complexes. Sample 2131 was passivated under conditions that should have ensured a mixture of N-2H and N-3H complexes, and as a result does not provide us with information on which complex the features might be. As explained above, for sample 2233 the discrepancies between the XSTM measurement, the PL data and the simulations of the passivation leave two scenarios open. Either only QW 1 is passivated, which could be with a mixture of N-2H and N-3H, or QW 1 is passivated with N-3H and QW 2 and 3 with N-2H. As a result, it is not possible to determine whether feature B and C are N-2H or N-3H related.

7.2.2 Empty State Imaging

Positive bias measurements on sample 2233 showed the typical wavefunctions of single N atoms in all QWs. Figure 7.9 shows such a measurement on QW 1 and 2, with QW 1 located on the left side of the image.

The observation of the wavefunctions of single N atoms in all QWs could mean that the wavefunction is not affected by the passivation, which is a surprising observation. Since the electronic influence of N in GaAs comes from the fact that states around the N atom are redistributed, one would expect that with the passivation of the atom, the states are somehow affected and the imaged wavefunction changes.

Another possibility is that not all the N atoms in the layer are passivated. This would mean that the observed wavefunctions originate from the non-passivated atoms. Because of the relatively high concentration of N in QW 1 (0.85 % as estimated by XRD) the wavefunctions show a lot of overlap. Even if they change or disappear after passivation, the contrast of the wavefunctions of the non-passivated N atoms dominates. We should also keep in mind that for feature C the hydrogen is easily removed by spectroscopy, as mentioned in 7.1.3. Measuring at positive bias might create the same circumstances that cause the NH-complex to disassociate, and as such it can be that feature C does not stay passivated during these measurements. Another possibility is that the cleaving of the sample breaks the passivation of some of the N atoms.

With the information available it is still undetermined if and how wavefunctions of a single N atoms change as a result of the passivation.

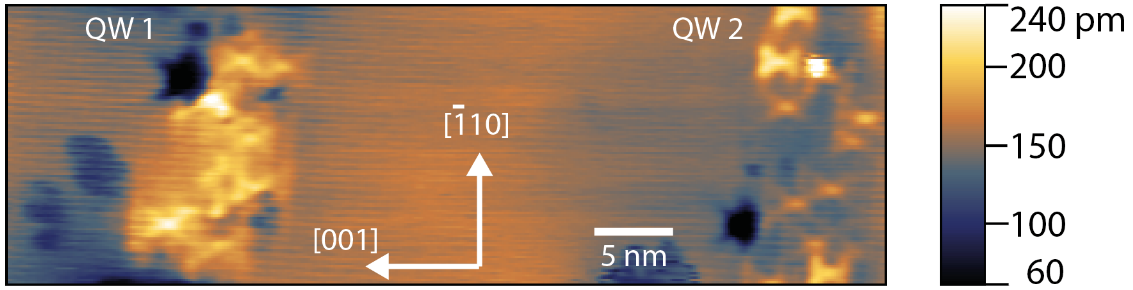

Figure 7.9: Empty stage image of QW 1 (left) and QW 2 (right) of sample 2233. Wavefunctions for N atoms in different layers can be observed in both QWs (1.8V 30pA 77K)

7.3 General Observations on Hydrogen Passivated N:GaAs

Aside from the features observed in the passivated N:GaAs layers, two other observations were made, not directly related to these features. These observations will be discussed here, as they provide useful information for future measurements.

The first observation is related to the structure of the sample and the quality of the cleaved surface. Non-passivated N:GaAs samples with a N concentration of up to 1.5 % usually cleave almost perfectly, with only a few atomic rows missing or left behind. For hydrogen passivated N:GaAs samples more cleavage induced defects are observed. The 1 % N concentration layer grown in the middle of sample 2233 negatively affected the quality of the cleave. The layer acted as a nucleation point for atomic steps that reached far into the area of QW 1, 2 and 3. This made high-resolution observation of these QWs more difficult. A possible explanation for this lies in the fact that passivated N atoms only have only have two remaining N-Ga bonds. While cleaving the sample, such an atom might be ripped out of the material more easily than a non-passivated N atom. In this way it can act as a nucleation point for larger cleavage induced defects.

The second observation is related the electronic properties of the grown layers. In the passivated N doped regions of both samples the conductivity at positive voltages is strongly reduced, as illustrated in Figure 7.10(a). This figure shows I/V measurements performed on sample 2131 in the passivated N:GaAs layer (black) and the GaAs buffer layer (red). To get an indication of the onset of the conductivity the absolute value of the IV spectrum is plotted with a logarithmic I-axis in Figure 7.10(b). Here it can been seen that the onset for tunneling into the conduction band is the same for the GaAs and the passivated N:GaAs. On the other side of the spectrum, the onset for tunneling from the valence band is about -0.9 V for the GaAs layer, while it is around -1.4 V for the passivated N:GaAs. GaAs layers that have been exposed to hydrogen show the same onset and conductivity characteristics as as-grown GaAs layers and non-passivated N:GaAs layers show the same characteristics as passivated N:GaAs layers. Earlier papers on STS measurements performed on non-passivated N:GaAs show an enhancement, instead of a decrease, of the conductivity close to the conduction band edge, caused by the N induced states [67] [61]. An explanation for why we did not observe this enhancement might be found in the cleavage induced defects. These are present throughout the sample and can cause a pinning of the Fermi level preventing us from probing the N induced states.

For large N:GaAs regions, such as in sample 2131, this created difficulties when trying to perform measurements at positive bias voltage, often resulting in the tip crashing. Both the passivated and non-passivated QWs of 2233 showed a decrease in conductivity at positive voltages. Here the effect was not as strong, likely related to the relatively thin N:GaAs layers and the presence of an undoped GaAs layer on either side. This enabled us to positive bias measurements without major issues on sample 2233.

Both of these observations need to be kept in mind when considering new N:GaAs sample designs.

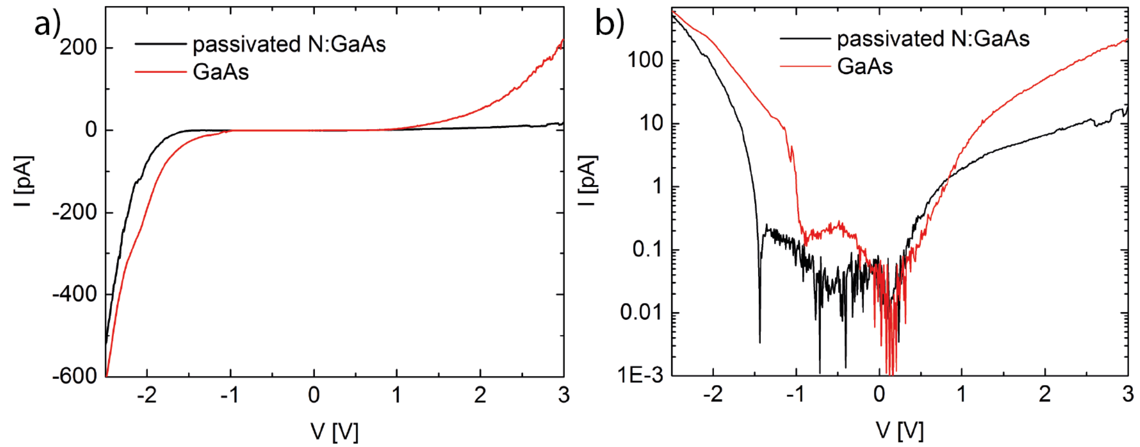

Figure 7.10: IV curves taken in N:GaAs layer and the GaAs buffer layer of sample 2131. (a) displays a linear plot of these spectra, while (b) shows a logarithmic plot of the absolute values.

7.4 Possible Lattice Orientations of the Observed Features

An in-depth understanding of the effect of passivation of N atoms on the observed STM contrast will require performing simulations such as DFT or tight-binding modeling, which is beyond the scope of this report. Instead we will consider possible lattice configurations of the NH complexes for the observed features. The depression of the surface observed for both feature B and C has very similar characteristics as a non-passivated 1st layer N atom. For the discussion in this section we will therefore assume that the passivated N atom of those features is located in the first layer. Such a first layer N atom is schematically displayed in Figure 7.11(a) by the green disc. The bonds of this atom are marked with the numbers 1 to 4. 1 is a dangling bond, 2 connects to a Ga atom in the underlying layer, and 3 and 4 connect to Ga atoms within the same layer and corrugation row.

7.4.1 Feature A

It has already been discussed in Section 7.1.1 that feature A is not related to a hydrogen complex. Nevertheless it is still interesting to consider how the N adsorbed on the surface causes the dumbbell shape observed for feature A.

The lobes of the dumbbell are located on two neighboring As sites in the same corrugation row. This could indicate that the N atom is residing above the Ga atom located between these two As atoms. The N atom might then cause the As atoms to move out of the surface a bit, creating the dumbbell structure.

A two-lobe structure has been observed before for Mn, Fe and Zn atoms in GaAs [68], where the contrast is actually a composite state caused by very fast switching between two states. Depending on the measurement conditions either the composite state or one of the two single states was observed. Although for feature A no indications for switching have been observed, it could be that at the measurement conditions used in this research the switching rate is too fast to be observed.

7.4.2 Feature B

Feature B1 and B2 are observed in equal amounts and considering that the location of the bright dot is mirror-symmetric with respect to the (001) axis, it is likely that the NH-complex involved has the same mirror symmetry. Since bonds 3 and 4 are mirror-symmetric with respect to the (001) axis, they are likely involved.The fact that feature B is much deeper than a 1st layer N atom makes it likely that bond 2 is still intact, keeping the N atom in place, and maybe even pulling it

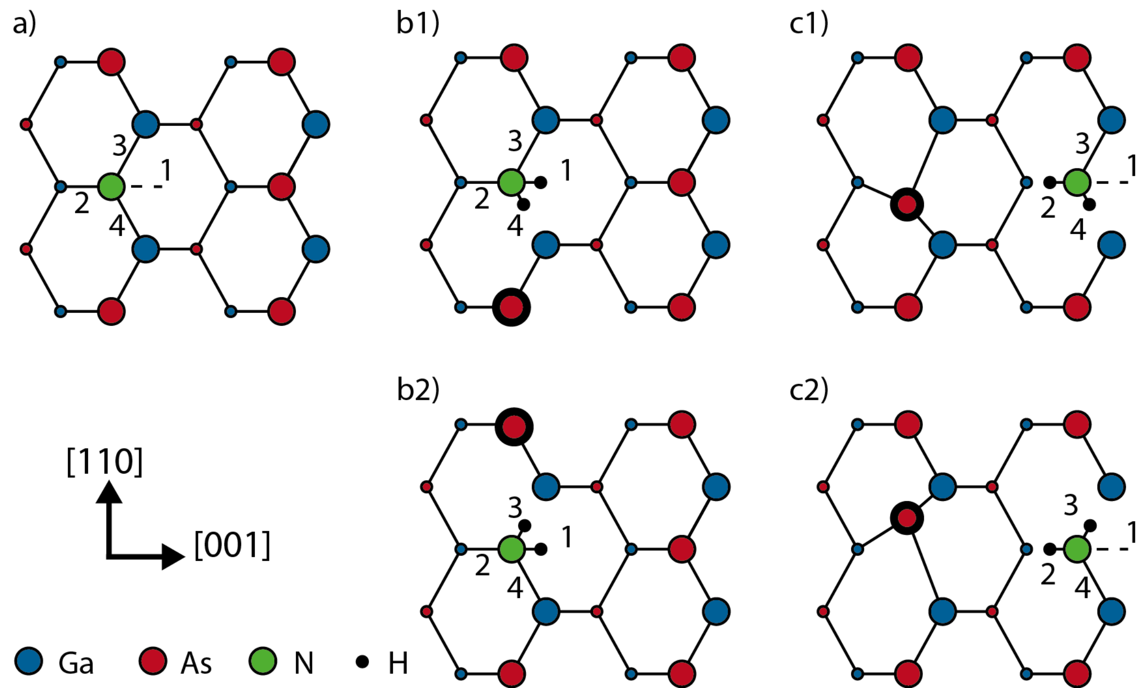

Figure 7.11: Schematic top view of the (110) surface. All five configurations contain a substitutional N atom in the first layer marked by the green disk. A non-passivated N atom is displayed in (a) with its bonds marked 1 to 4. Bond 1 is a dangling bond, oriented out of the surface. A possible configuration of the NH-complex of feature B1 and B2 is displayed in (b1) and (b2) respectively. The As atom with the thicker circle is the one expected to relax outwards to create the bright contrast as observed in feature B. (c1)/(c2) A possible configuration for feature C1 and C2 respectively. The As atom with the thicker circle again marks the one expected to relax outwards. For the configurations of both feature B(1/2) and feature C(1/2) it has not been considered on which side the As atom relaxes. Therefore, in all configurations where bond 3 is broken, it could be that bond 4 is broken instead and vice versa.

further down due to the breaking of bond 3 or 4. Following the theory that two N-Ga are broken in the NH-complexes, this would leave bond 1 as the other hydrogen terminated bond in feature B.

The suggested orientations of complex B1 and B2 are displayed in Figure 7.11(b1) and (b2) respectively, where the small black discs mark the H atoms and the As atom with the thicker black circle marks the As atom that relaxes out of the surface to create the bright contrast of feature B. Whether the relaxation of the As atom in Figure 7.11(b1) is caused by the breaking of bond 3 or bond 4 was deemed too complex to consider. In other words, whether the breaking of bond 3 causes a relaxation of the As atom in the same direction relative to the N atom ([110]) or in the opposite direction of the N atom ([$\bar{1}\bar{1}$0]). As a result it could be that bond 4 is broken instead of bond 3 to create feature B1.

This description does not take into account the asymmetry that might exist in the depth of B1 and B2 as mentioned in Section 7.1.2. If B1 and B2 are N-3H complexes, the third hydrogen atom could be the cause of this asymmetry.

7.4.3 Feature C

In feature C the bright dot shows up in the neighboring corrugation row, thus it is seems reasonable to assume that bond 2 is broken by the passivation. This could allow the As atom in neighboring row to relax outwards a bit and let the N atom relax upwards. This would agree with the observation from Section 7.1.3 that feature C is slightly less deep than a normal N atom in the first layer. This leaves us to speculate which other bond is involved to make the N-2H complex. Considering the mirror-symmetric orientation of C1 and C2, bond 3 and 4 might be involved again. This matches with the observation that C1 and C2 occur with the same frequency, but leaves the N atom with only one remaining bond to the crystal, which could make it unstable. How the relaxation of the lattice, due to the breaking of bond 3 or 4, propagates into the neighboring corrugation row is considered to be too complex to discuss without proper simulations.

This suggested orientation for feature C is displayed in Figure 7.11(c). Once again the small black discs mark the H atoms and the As atom with the thicker circle marks the atom that relaxes outwards to create the bright contrast of feature C. Whether the direction of the relaxation of the As atom in Figure 7.11(c1) should be in the [$\bar{1}\bar{1}$0] direction (as imaged) or in the [110] direction was deemed too complex to consider. As a result it could be that the imaged relaxation in Figure 7.11(c1) is caused by the breaking of bond 4.

Another possibility for feature C is that, instead of bond 3 or 4, bond 1 is the second passivated bond. This orientation is not displayed, but only discussed in text. This would mean that the N atom is still fully connected to its own corrugation row. The As atom in the neighboring row would still be able to relax outwards, since it is not connected to the N atom anymore. This lattice configuration is fully symmetric with respect to the [001] axis. To create the observed features C1 and C2, the complex might relax to a canted configuration, causing the relaxed As atom to move as well.

This configuration does however not match with the current interpretation of feature B, which involves either bond 1 and 3, or 1 and 4. Assuming that each bond has an equal chance of being passivated, each combination of two bonds should have the same chance to form the NH-complex. Since this second interpretation of feature C involves only bond 1 and 2 its chance to occur should be equal to either configuration of feature B. Meaning that when counting the observed features in a passivated layer we should find twice the number of feature B when compared to feature C. Instead, we observed equal amount of feature B and C. As a result, this second interpretation of the orientation of feature C is mutually exclusive with the current interpretation of feature B.

7.5 Conclusion

With XSTM measurements performed on hydrogen passivated N:GaAs we observed features never seen on non-passivated N:GaAs. We identified three main types of features and named them A,

B(1/2) and C(1/2). Feature A has a dumbbell-like shape and is attributed to a N atom adsorbed on the surface. This feature can move over the surface under normal scanning conditions.

Feature B and C are related to NH-complexes. Both NH features can be switched or modified by taking spectroscopy curves at their location. Feature B can be switched from B1 to B2 and vice versa by taking spectroscopy measurements at its location. Feature C loses the bright dot, visible in the next corrugation row, when performing spectroscopy. The fact that for feature C the bright dot can be removed, while in feature B it can only switch its position in the lattice, points to a greater bonding strength of feature B. Whether feature B and C are N-2H or N-3H related cannot be said with certainty without further research.

Regarding general observations on hydrogen passivated N:GaAs samples, we observed that the passivated layers contained more cleavage induced artifacts than usually observed in N:GaAs samples. This could be caused by the passivation, leaving N atoms with only two N-Ga bonds. During cleaving these atoms can more easily break from the crystal, and act as a nucleation point for larger cleavage induced artifacts.

We also considered, without performing any calculations like DFT or tight-binding modeling, the possible configuration of the NH-complexes that might cause observed contrast of feature A, B and C. While some considered scenarios seem plausible, it is impossible to say if they are correct without performing in-depth calculations on these crystal configurations.

7.6 Outlook

While some fascinating observations were made on the passivated N:GaAs samples, there are still quite a few things unknown about the observed features. The question whether feature B and C are N-2H or N-3H related can be answered by measurements on a sample that is passivated under circumstances that promote the formation of N-2H complexes. This sample should also provide information on whether N-2H complexes can be observed at all with STM. Regarding the contrast of B and C, it would be interesting to perform DFT calculations on the possible NH-complexes and simulate the STM contrast of these. This should also provide insight on the exact atomic configuration of the complexes. On the subject of new sample designs, two things should be kept in mind. First of all we should avoid thick regions of high (>1%) N concentration to reduce cleavage induced defects and also to retain conductivity at positive voltages. Secondly, if we want to observe if, and how, the wavefunctions of passivated N atoms change, the N concentration should be kept very low. This to avoid that the wavefunctions of different N atoms show to much overlap.

Chapter 8

Conclusions and Outlook

We exposed a N:GaAs and a Sb:GaAs sample to a hydrogen plasma to try and passivate them. After the first exposure weak indications of passivation are observed in both samples by PL and XRD-RC measurements. For the N:GaAs sample the indications for passivation are a 4 times decrease in the ratio between the GaAs and N:GaAs PL peak, and a vague shoulder appearing in the XRD-RC measurement. For the Sb:GaAs sample the indication for passivation is a decrease in the distance between the GaAs and Sb:GaAs peak. A second exposure, with a higher hydrogen dose, has likely damaged the samples, causing a complete disappearance of the N and Sb peaks in XRD-RC measurements. In PL this is visible in both samples by the disappearance of the GaAs and N/Sb:GaAs peaks and the appearance of a single peak around 860 nm. Thermal annealing was performed on the samples after the second hydrogen exposure. Annealing at 250°C showed a decrease in PL intensity of an order of magnitude, but has little effect on the peak position. The 330°C annealing caused a blueshift of the PL peak to around 845 nm in both samples. In the Sb:GaAs a broad peak appeared around 950 nm, which might originate from remaining Sb, but further research needs to be done to gain a better insight in this.

To check whether the samples have been damaged by the second hydrogen exposure, we can compare the surface of these samples with the reference samples. This could easily be done with an optical microscopy, but for a more detailed view scanning electron microscopy would be good option. For a new hydrogen passivation run it is interesting to repeat the conditions of the first exposure, but extend the time by a few hours. Because we observed indications of partial passivation with a 1 hour exposure, longer exposures might make these indications more significant. Since the annealing at 330°C had a larger effect, it would be interesting to perform this annealing for a longer time and see what the effects are. By doing this on the same samples we can try to obtain a general trend in the changes in the spectra during the annealing. With this we could also check if the broad PL peak around 950 nm in the Sb:GaAs samples gets more pronounced.

With XSTM measurements performed on hydrogen passivated N:GaAs we observed features never seen on non-passivated N:GaAs. We identified three main types of features and named them A, B(1/2) and C(1/2). Feature A has a dumbbell-like shape and is attributed to a N atom adsorbed on the surface. This feature can move over the surface under normal scanning conditions.

Feature B and C are related to NH-complexes. Both NH features can be switched or modified by taking spectroscopy curves at their location. Feature B can be switched from B1 to B2 and vice versa by taking spectroscopy measurements at its location. Feature C loses the bright dot, visible in the next corrugation row, when performing spectroscopy. The fact that for feature C the bright dot can be removed, while in feature B it can only switch its position in the lattice, points to a greater bonding strength of feature B. Whether feature B and C are N-2H or N-3H related cannot be said with certainty without further research.

Regarding general observations on hydrogen passivated N:GaAs samples, we observed that the passivated layers contained more cleavage induced artifacts than usually observed in N:GaAs samples. This could be caused by the passivation, leaving N atoms with only two N-Ga bonds.

During cleaving these atoms can more easily break from the crystal, and act as a nucleation point for larger cleavage induced artifacts.

We also considered, without performing any calculations like DFT or tight-binding modeling, the possible configuration of the NH-complexes that might cause observed contrast of feature A, B and C. While some considered scenarios seem plausible, it is impossible to say if they are correct without performing in-depth calculations on these crystal configurations.

While some fascinating observations were made on the passivated N:GaAs samples, there are still quite a few things unknown about the observed features. The question whether feature B and C are N-2H or N-3H related can be answered by measurements on a sample that is passivated under circumstances that promote the formation of N-2H complexes. This sample should also provide information on whether N-2H complexes can be observed at all with STM. Regarding the contrast of B and C, it would be interesting to perform DFT calculations on the possible NH-complexes and simulate the STM contrast of these. This should also provide insight on the exact atomic configuration of the complexes. On the subject of new sample designs, two things should be kept in mind. First of all we should avoid thick regions of high (>1%) N concentration to reduce cleavage induced defects and also to retain conductivity at positive voltages. Secondly, if we want to observe if, and how, the wavefunctions of passivated N atoms change, the N concentration should be kept very low. This to avoid that the wavefunctions of different N atoms show to much overlap.

Bibliography

[1] M Haurylau, G Chen, H Chen, J Zhang, NA Nelson, DH Albonesi, EG Friedman, and PM Fauchet. On-chip optical interconnect roadmap: challenges and critical directions. *IEEE Journal of Selected Topics in Quantum Electronics*, 12(6):1699–1705, 2006. 1

[2] P Lodahl, S Mahmoodian, and S Stobbe. Interfacing single photons and single quantum dots with photonic nanostructures. *Reviews of Modern Physics*, 87(2):347, 2015. 1

[3] A Mohan, P Gallo, M Felici, B Dwir, A Rudra, J Faist, and E Kapon. Record-low inhomogeneous broadening of site-controlled quantum dots for nanophotonics. *Small*, 6(12):1268–1272, 2010. 1

[4] G Pettinari, A Gerardino, L Businaro, A Polimeni, M Capizzi, M Hopkinson, S Rubini, F Biccari, F Intonti, A Vinattieri, et al. A lithographic approach for quantum dot-photonic crystal nanocavity coupling in dilute nitrides. *Microelectronic Engineering*, 174:16–19, 2017. 1

[5] D Leonard, M Krishnamurthy, CMv Reaves, SP DenBaars, and PM Petroff. Direct formation of quantum-sized dots from uniform coherent islands of InGaAs on GaAs surfaces. *Applied Physics Letters*, 63(23):3203–3205, 1993. 1

[6] S Figge, C Tessarek, T Aschenbrenner, and D Hommel. InGaN quantum dot growth in the limits of Stranski-Krastanov and spinodal decomposition. *physica status solidi (b)*, 248(8):1765–1776, 2011. 1

[7] Á Nemcsics. Quantum dots prepared by droplet epitaxial method. 2015. 1

[8] C Schneider, A Huggenberger, T Sünner, T Heindel, M Strauß, S Göpfert, P Weinmann, S Reitzenstein, L Worschech, M Kamp, et al. Single site-controlled In(Ga)As/GaAs quantum dots: growth, properties and device integration. *Nanotechnology*, 20(43):434012, 2009. 1

[9] F Biccari, A Boschetti, G Pettinari, F La China, M Gurioli, F Intonti, A Vinattieri, MS Sharma, M Capizzi, A Gerardino, L Businaro, M Hopkinson, A Polimeni, and M Felici. Site-controlled single-photon emitters fabricated by near-field illumination. *Advanced Materials*, 30(21):1705450, 2018. 1, 6

[10] M Felici, G Pettinari, F Biccari, M Capizzi, and A Polimeni. Spatially selective hydrogen irradiation of dilute nitride semiconductors: a brief review. *Semiconductor Science and Technology*, 33(5):053001, 2018. 1

[11] N Balakrishnan, A Patanè, O Makarovsky, A Polimeni, M Capizzi, F Martelli, and S Rubini. Laser writing of the electronic activity of N- and H-atoms in gaas. *Applied Physics Letters*, 99(2):021105, 2011. 1, 6

[12] N Balakrishnan, G Pettinari, O Makarovsky, L Turyanska, MW Fay, M De Luca, A Polimeni, M Capizzi, F Martelli, S Rubini, et al. Band-gap profiling by laser writing of hydrogen-containing III-N-Vs. *Physical Review B*, 86(15):155307, 2012. 1, 6

[13] G Pettinari, M Felici, R Trotta, M Capizzi, and A Polimeni. Hydrogen effects in dilute III-N-V alloys: From defect engineering to nanostructuring. *Journal of Applied Physics*, 115(1):012011, 2014. 1

[14] FJ Tilley, M Roy, PA Maksym, PM Koenraad, CM Krammel, and JM Ulloa. Scanning tunneling microscopy contrast of isovalent impurities on the GaAs (110) surface explained with a geometrical model. *Physical Review B*, 93(3):035313, 2016. 2, 11

[15] CM Krammel, M Roy, FJ Tilley, PA Maksym, LY Zhang, P Wang, K Wang, YY Li, SM Wang, and PM Koenraad. Incorporation of Bi atoms in InP studied at the atomic scale by cross-sectional scanning tunneling microscopy. *Physical Review Materials*, 1(3):034606, 2017. 2

[16] JM Ulloa, PM Koenraad, and M Hopkinson. Structural properties of GaAsN/GaAs quantum wells studied at the atomic scale by cross-sectional scanning tunneling microscopy. *Applied Physics Letters*, 93(8):083103, 2008. 2, 11, 29

[17] RC Plantenga, VR Kortan, T Kaizu, Y Harada, T Kita, ME Flatté, and PM Koenraad. Spatially resolved electronic structure of an isovalent nitrogen center in GaAs. *Physical Review B*, 96(15):155210, 2017. 2, 11, 12, 29

[18] I Vurgaftman, J Meyer, and L Ram-Mohan. Band parameters for III-V compound semiconductors and their alloys. *Journal of applied physics*, 89(11):5815–5875, 2001. 3

[19] M Weyers, M Sato, and H Ando. Red shift of photoluminescence and absorption in dilute GaAsN alloy layers. *Japanese Journal of Applied Physics*, 31(7A):L853, 1992. 3

[20] W Shan, W Walukiewicz, JW Ager III, EE Haller, JF Geisz, DJ Friedman, JM Olson, and SR Kurtz. Band anticrossing in GaInNAs alloys. *Physical Review Letters*, 82(6):1221, 1999. 3

[21] W Shan, W Walukiewicz, JW Ager III, EE Haller, JF Geisz, DJ Friedman, JM Olson, and SR Kurtz. Effect of nitrogen on the band structure of GaInNAs alloys. *Journal of applied physics*, 86(4):2349–2351, 1999. 3

[22] J Yoshida, T Kita, O Wada, and K Oe. Temperature dependence of $GaAs_{1-x}Bi_x$ band gap studied by photoreflectance spectroscopy. *Japanese journal of applied physics*, 42(2R):371, 2003. 3

[23] M De la Mare, Q Zhuang, A Krier, A Patanè, and S Dhar. Growth and characterization of InAsN/GaAs dilute nitride semiconductor alloys for the midinfrared spectral range. *Applied Physics Letters*, 95(3):031110, 2009. 3

[24] IC Sandall, F Bastiman, B White, R Richards, D Mendes, JPR David, and CH Tan. Demonstration of InAsBi photoresponse beyond 3.5 μm. *Applied Physics Letters*, 104(17):171109, 2014. 3

[25] HP Hjalmarson, P Vogl, DJ Wolford, and JD Dow. Theory of substitutional deep traps in covalent semiconductors. *Physical Review Letters*, 44(12):810, 1980. 3

[26] J Wu, W Shan, and W Walukiewicz. Band anticrossing in highly mismatched III-V semiconductor alloys. *Semiconductor Science and Technology*, 17(8):860, 2002. 3, 4

[27] K Alberi, J Wu, W Walukiewicz, KM Yu, OD Dubon, SP Watkins, CX Wang, X Liu, Y-J Cho, and J Furdyna. Valence-band anticrossing in mismatched III-V semiconductor alloys. *Physical review B*, 75(4):045203, 2007. 3

[28] SJ Pearton, JW Corbett, and TS Shi. Hydrogen in crystalline semiconductors. *Applied Physics A*, 43(3):153–195, 1987. 4

[29] S Mo Myers, MI Baskes, HK Birnbaum, Jo Wo Corbett, GG DeLeo, SK Estreicher, Eo E Haller, Po Jena, No M Johnson, Ro Kirchheim, et al. Hydrogen interactions with defects in crystalline solids. *Reviews of Modern Physics*, 64(2):559, 1992. 4, 26, 27

[30] C Dube and JI Hanoka. Hydrogen passivation of dislocations in silicon. *Applied Physics Letters*, 45(10):1135–1137, 1984. 4

[31] CG Van de Walle and BR Tuttle. Microscopic theory of hydrogen in silicon devices. *IEEE Transactions on Electron Devices*, 47(10):1779–1786, 2000. 4

[32] A Polimeni, M Bissiri, M Felici, M Capizzi, IA Buyanova, WM Chen, HP Xin, and CW Tu. Nitrogen passivation induced by atomic hydrogen: The $GaP_{1-y}N_y$ case. *Physical Review B*, 67(20):201303, 2003. 4

[33] A Polimeni, F Masia, M Felici, G Baldassarri Höger von Högersthal, M Bissiri, A Frova, M Capizzi, PJ Klar, W Stolz, IA Buyanova, et al. Hydrogen-related effects in diluted nitrides. *Physica B: Condensed Matter*, 340:371–376, 2003. 4

[34] G Pettinari, A Patanè, A Polimeni, M Capizzi, Xianfeng Lu, and T Tiedje. Effects of hydrogen on the electronic properties of Ga(AsBi) alloys. *Applied Physics Letters*, 101(22):222103, 2012. 4

[35] G Luo, S Yang, GR Jenness, Z Song, TF Kuech, and D Morgan. Understanding and reducing deleterious defects in the metastable alloy GaAsBi. *NPG Asia Materials*, 9(1), 2017. 4

[36] S Birindelli, M Kesaria, D Giubertoni, G Pettinari, AV Velichko, QD Zhuang, A Krier, A Patanè, A Polimeni, and M Capizzi. Peculiarities of the hydrogenated In(AsN) alloy. *Semiconductor Science and Technology*, 30(10):105030, 2015. 4

[37] L Wen, M Stavola, WB Fowler, R Trotta, A Polimeni, M Capizzi, G Bisognin, M Berti, S Rubini, and F Martelli. Microscopic origin of compressive strain in hydrogen-irradiated dilute $GaAs_{1-y}N_y$ alloys: Role of NH_n centers with $n > 2$ and their thermal stability. *Physical Review B*, 86(8):085206, 2012. 4, 5

[38] A Polimeni, HM Bissiri, M Capizzi, M Fischer, M Reinhardt, A Forchel, et al. Effect of hydrogen on the electronic properties of $In_xGa_{1-x}As_{1-y}N_y$ GaAs quantum wells. *Physical Review B*, 63(20):201304, 2001. 4

[39] G Baldassarri H. v. H, M Bissiri, A Polimeni, M Capizzi, M Fischer, M Reinhardt, and A Forchel. Hydrogen-induced band gap tuning of (InGa)(AsN)/GaAs single quantum wells. *Applied Physics Letters*, 78(22):3472–3474, 2001. 4

[40] R Trotta, D Giubertoni, A Polimeni, M Bersani, M Capizzi, F Martelli, S Rubini, G Bisognin, and M Berti. Hydrogen diffusion in $GaAs_{1-x}N_x$. *Physical Review B*, 80(19):195206, 2009. 4, 20

[41] M Bissiri, G Baldassarri Höger von Högersthal, A Polimeni, V Gaspari, F Ranalli, M Capizzi, A Amore Bonapasta, F Jiang, M Stavola, D Gollub, et al. Hydrogen-induced passivation of nitrogen in $GaAs_{1-y}N_y$. *Physical Review B*, 65(23):235210, 2002. 4

[42] G Bisognin, D De Salvador, AV Drigo, E Napolitani, A Sambo, M Berti, A Polimeni, M Felici, M Capizzi, M Güngerich, et al. Hydrogen-nitrogen complexes in dilute nitride alloys: Origin of the compressive lattice strain. *Applied physics letters*, 89(6):061904, 2006. 4

[43] A Amore Bonapasta, F Filippone, P Giannozzi, M Capizzi, and A Polimeni. Structure and passivation effects of mono-and dihydrogen complexes in $GaAs_yN_{1-y}$ alloys. *Physical review letters*, 89(21):216401, 2002. 4

[44] F Jiang, M Stavola, M Capizzi, A Polimeni, A Amore Bonapasta, and F Filippone. Vibrational spectroscopy of hydrogenated $GaAs_{1-y}N_y$: A structure-sensitive test of an $H_2^*(N)$ model. *Physical Review B*, 69(4):041309, 2004. 4

[45] G Ciatto, F Boscherini, A Amore Bonapasta, F Filippone, A Polimeni, and M Capizzi. Nitrogen-hydrogen complex in $GaAs_xN_{1-x}$ revealed by x-ray absorption spectroscopy. *Physical Review B*, 71(20):201301, 2005. 4

[46] G Ciatto, F Boscherini, A Amore Bonapasta, F Filippone, A Polimeni, M Capizzi, M Berti, G Bisognin, D De Salvador, L Floreano, et al. Local structure of nitrogen-hydrogen complexes in dilute nitrides. *Physical Review B*, 79(16):165205, 2009. 4

[47] L Wen, F Bekisli, M Stavola, WB Fowler, R Trotta, Antonio Polimeni, M Capizzi, S Rubini, and F Martelli. Detailed structure of the H-N-H center in $GaAs_yN_{1-y}$ revealed by vibrational spectroscopy under uniaxial stress. *Physical Review B*, 81(23):233201, 2010. 4

[48] G Bisognin, D De Salvador, E Napolitani, M Berti, A Polimeni, M Capizzi, S Rubini, F Martelli, and A Franciosi. High-resolution X-ray diffraction in situ study of very small complexes: the case of hydrogenated dilute nitrides. *Journal of Applied Crystallography*, 41(2):366–372, 2008. 4, 26

[49] L Amidani, G Ciatto, F Boscherini, F Filippone, G Mattioli, P Alippi, F Bondino, A Polimeni, M Capizzi, and A Amore Bonapasta. Connections between local and macroscopic properties in solids: The case of N in III-V-N alloys. *Physical Review B*, 89(8):085301, 2014. 5

[50] M Berti, G Bisognin, D De Salvador, E Napolitani, S Vangelista, A Polimeni, M Capizzi, F Boscherini, G Ciatto, S Rubini, et al. Formation and dissolution of DN complexes in dilute nitrides. *Physical Review B*, 76(20):205323, 2007. 5, 26

[51] R Trotta, A Polimeni, F Martelli, G Pettinari, M Capizzi, L Felisari, S Rubini, M Francardi, A Gerardino, PCM Christianen, et al. Fabrication of site-controlled quantum dots by spatially selective incorporation of hydrogen in Ga(AsN)/GaAs heterostructures. *Advanced Materials*, 23(24):2706–2710, 2011. 6

[52] G Binnig, H Rohrer, C Gerber, and E Weibel. Surface studies by scanning tunneling microscopy. *Physical review letters*, 49(1):57, 1982. 7

[53] J Bardeen. Tunnelling from a many-particle point of view. *Physical Review Letters*, 6(2):57, 1961. 8

[54] J Tersoff and DR Hamann. Theory of the scanning tunneling microscope. In *Scanning Tunneling Microscopy*, pages 59–67. Springer, 1985. 9

[55] M Sabisch, P Krüger, and J Pollmann. Ab initio calculations of SiC (110) and GaAs (110) surfaces: A comparative study and the role of ionicity. *Physical Review B*, 51(19):13367, 1995. 10

[56] JR Chelikowsky, SG Louie, and ML Cohen. Relaxation effects on the (110) surface of gaas. *Physical Review B*, 14(10):4724, 1976. 10

[57] JR Chelikowsky and ML Cohen. Self-consistent pseudopotential calculation for the relaxed (110) surface of GaAs. *Physical Review B*, 20(10):4150, 1979. 10

[58] Z Li, H Chen, F Kong, Q Sun, and Y Kawazoe. Relaxations of nonpolar zinc blende (110) surface of GaN, AlN, and BN. *Journal of applied physics*, 84(4):1977–1980, 1998. 10

[59] HA McKay, RM Feenstra, T Schmidtling, and UW Pohl. Arrangement of nitrogen atoms in GaAsN alloys determined by scanning tunneling microscopy. *Applied Physics Letters*, 78(1):82–84, 2001. 11, 29

[60] HA McKay, RM Feenstra, T Schmidtling, UW Pohl, and JF Geisz. Distribution of nitrogen atoms in dilute GaAsN and InGaAsN alloys studied by scanning tunneling microscopy. *Journal of Vacuum Science & Technology B: Microelectronics and Nanometer Structures Processing, Measurement, and Phenomena*, 19(4):1644–1649, 2001. 11, 29

[61] N Ishida, M Jo, T Mano, Y Sakuma, T Noda, and D Fujita. Direct visualization of the n impurity state in dilute GaNAs using scanning tunneling microscopy. *Nanoscale*, 7(40):16773–16780, 2015. 11, 29, 32, 37

[62] RM Feenstra, G Meyer, F Moresco, and KH Rieder. Low-temperature scanning tunneling spectroscopy of n-type GaAs (110) surfaces. *Physical Review B*, 66(16):165204, 2002. 13

[63] RM Feenstra, JA Stroscio, and AP Fein. Tunneling spectroscopy of the Si (111) 2×1 surface. *Surface science*, 181(1-2):295–306, 1987. 14

[64] A Wijnheijmer. Manipulation and analisys of a single dopant atom in GaAs, 2011. 15

[65] DJ Sharp, JKG Panitz, and DM Mattox. Applications of a Kaufman ion source to low energy ion erosion studies. *Journal of Vacuum Science and Technology*, 16(6):1879–1882, 1979. 19

[66] S Tanaka, H Kobayashi, H Saito, and S Shionoya. Luminescence of high density electron-hole plasma in GaAs. *Journal of the Physical Society of Japan*, 49(3):1051–1059, 1980. 24

[67] L Ivanova, H Eisele, MP Vaughan, Ph Ebert, A Lenz, R Timm, O Schumann, L Geelhaar, M Dahne, S Fahy, et al. Direct measurement and analysis of the conduction band density of states in diluted $GaAs_{1-x}N_x$ alloys. *Physical Review B*, 82(16):161201, 2010. 37

[68] A Richardella, D Kitchen, and A Yazdani. Mapping the wave function of transition metal acceptor states in the GaAs surface. *Physical Review B*, 80(4):045318, 2009. 38